Senescence-inducing stress promotes proteolysis of phosphoglycerate mutase via ubiquitin ligase Mdm2

Takumi Mikawa,[1] Takeshi Maruyama,[1] Koji Okamoto,[3] Hitoshi Nakagama,[3] Matilde E. Lleonart,[4] Takeshi Tsusaka,[1] Kousuke Hori,[1] Itsuo Murakami,[1] Taisuke Izumi,[5] Akifumi Takaori-Kondo,[2] Masayuki Yokode,[6] Gordon Peters,[7] David Beach,[8] and Hiroshi Kondoh[1]

[1]Department of Geriatric Medicine and [2]Department of Hematology/Oncology, Graduate School of Medicine, Kyoto University, Kyoto 606-8507, Japan
[3]Division of Cancer Development System, National Cancer Center Research Institute, Tsukiji, Tokyo 104-0045, Japan
[4]Department of Pathology, Hospital Vall de'Hebron, 08035 Barcelona, Spain
[5]Viral Mutation Section, HIV Drug Resistance Program, National Cancer Institute, Frederick National Laboratory for Cancer Research, Frederick, MD 21702
[6]Department of Clinical Innovative Medicine, Translational Research Center, Kyoto University Hospital, Kyoto 606-8507, Japan
[7]Cancer Research UK, London Research Institute, London WC2A 3LY, England, UK
[8]Center for Cutaneous Biology, Institute for Cell and Molecular Science, London UK E1 2AT, England, UK

Despite the well-documented clinical significance of the Warburg effect, it remains unclear how the aggressive glycolytic rates of tumor cells might contribute to other hallmarks of cancer, such as bypass of senescence. Here, we report that, during oncogene- or DNA damage–induced senescence, Pak1-mediated phosphorylation of phosphoglycerate mutase (PGAM) predisposes the glycolytic enzyme to ubiquitin-mediated degradation. We identify Mdm2 as a direct binding partner and ubiquitin ligase for PGAM in cultured cells and in vitro. Mutations in PGAM and Mdm2 that abrogate ubiquitination of PGAM restored the proliferative potential of primary cells under stress conditions and promoted neoplastic transformation. We propose that Mdm2, a downstream effector of p53, attenuates the Warburg effect via ubiquitination and degradation of PGAM.

Introduction

Enhanced glycolysis is a characteristic feature of cancerous cells and tissues, commonly referred to as the Warburg effect (Warburg, 1956). This property is used in clinical practice for the detection of metastatic tumor mass by positron-emission scanning of 2-[^{18}F]fluoro-2-deoxy-D-glucose. It has been widely assumed that cancer cells maintain up-regulated glycolytic metabolism to adapt to the hypoxic conditions in vivo, as solid aggressive tumors overgrow the blood supply of the feeding neovasculature.

Enhanced glycolysis under hypoxic conditions is mediated in part by activation of hypoxia-inducible transcription factor (HIF-1), which directly regulates most of the glycolytic enzymes (Iyer et al., 1998). In such a context, the glycolytic response represents a successful metabolic adaptation of cancer cells in vivo. However, the Warburg effect cannot be simply explained by cellular adaptation to hypoxia, as cancer cells maintain enhanced glycolysis even in standard tissue culture conditions (20% oxygen) and in circulating cancers (Koppenol et al., 2011). A more plausible rationalization is that it enables cancer cells to meet their requirements for both energy and metabolic precursors for biosynthesis (Vander Heiden et al., 2009).

We recently reported an intriguing relationship between the glycolytic pathway and cellular senescence (Kondoh et al., 2005). All primary somatic cells, with the exception of pluripotent stem cells, have a limited replicative capacity under standard tissue culture conditions and suffer a permanent cell cycle arrest, called replicative senescence (Hayflick, 1965). The senescent phenotype can also manifest prematurely, upon exposure to oncogenic mutation (Serrano et al., 1997), oxidative stress (Parrinello et al., 2003), DNA damage (Chen and Ames, 1994), and secreted cytokines (Acosta et al., 2008; Kuilman et al., 2008; for review see Campisi, 2013). Glycolytic flux declines during

T. Mikawa and T. Maruyama contributed equally to this paper.

Correspondence to Hiroshi Kondoh: hkondoh@kuhp.kyoto-u.ac.jp

Abbreviations used in this paper: DKO, double knockout; MEF, mouse embryonic fibroblast; PGAM, phosphoglycerate mutase; SA-β-Gal, senescence-associated β-galactosidase; SIS, stress-induced senescence.

The Rockefeller University Press $30.00
J. Cell Biol. Vol. 204 No. 5 729–745
www.jcb.org/cgi/doi/10.1083/jcb.201306149

senescence in mouse and human primary cells (Zwerschke et al., 2003; Kondoh et al., 2005), and inhibition of glycolytic flux provokes premature senescence (Kondoh et al., 2005).

A key finding in this regard was the identification of phosphoglycerate mutase (PGAM), the enzyme that converts 3-phosphoglycerate to 2-phosphoglycerate in the glycolytic pathway, in an unbiased genetic screen for bypass of senescence in mouse embryonic fibroblasts (MEFs; Kondoh et al., 2005). Conversely, MJE3, a compound identified in a chemical genomics screen for inhibitors of breast cancer cell proliferation, was shown to specifically target PGAM (Evans et al., 2005). PGAM activity is up-regulated in many cancerous tissues, including tumors of the lung, colon, liver, and breast (Durany et al., 1997, 2000; Ren et al., 2010). Indeed, a cancer-specific isoform of pyruvate kinase, designated M2, activates an alternative glycolytic pathway in cancer cells accompanied by dramatic enhancement of PGAM activity (Vander Heiden et al., 2010). As recent results suggest, the pivotal role of PGAM in coordinating glycolysis and biosynthesis make it an attractive target for therapeutic intervention (Hitosugi et al., 2012).

Despite our enhanced understanding of how PGAM regulates glycolysis, rather little is known about the regulation of PGAM. PGAM is the only glycolytic enzyme that is not transcriptionally controlled by HIF-1 (Iyer et al., 1998). Although the muscle-specific form of PGAM can be activated by p53 (Ruiz-Lozano et al., 1999), there is currently no evidence that PGAM is transcriptionally altered during tumorigenesis. Recent findings instead suggest that PGAM activity is regulated posttranscriptionally. For example, phosphorylation of PGAM by p21 (Cdc42/Rac1)-activated kinase1 (Pak1) results in loss of activity (Shalom-Barak and Knaus, 2002), but the precise mechanism and relevance remains unknown. Here we show that during oncogene-induced senescence or other forms of stress-induced senescence (SIS), Pak1-mediated phosphorylation of PGAM provokes its ubiquitination and turnover. The ubiquitin ligase MDM2, a transcriptional target of p53, binds to and ubiquitinates PGAM in a phosphorylation-dependent manner. Of particular note, ubiquitin site mutations in PGAM stabilize the protein and sustain cellular proliferation under stress conditions.

Results

Ubiquitin-dependent degradation of PGAM during SIS

Having previously shown that PGAM can bypass replicative senescence (Kondoh et al., 2005), we were interested to know what happens to PGAM levels and activity in MEFs undergoing oncogene-induced senescence or SIS. There are two reported isoforms of *PGAM—PGAM1* (brain form) and *PGAM2* (muscle form)—whose cDNA sequences are 79% and 81% identical in mouse and human cells, respectively. Although the respective homodimers predominate in specific cell types, most normal mouse tissues contain heterodimers of PGAM-1 and -2 (Zhang et al., 2001). Consistent with this study, we found that the levels of *PGAM2* mRNA are almost equivalent to or exceed those of *PGAM1* mRNA in some mouse tissues (skin, bone, and lung), whereas *PGAM1* mRNA is predominant in others (blood vessel, white adipose tissue, and liver; Fig. S1 A). Moreover, they have similar enzymatic activities and show similar effects on glycolytic flux when overexpressed in MEFs (Fig. S1 B). We generated polyclonal antiserum against recombinant PGAM2, and although it was affinity-purified using mouse PGAM2 protein, it was found to recognize both isoforms of the mouse and human PGAM proteins (Fig. S1, C–F).

To induce SIS, we exposed primary MEFs to low doses of etoposide (Chen and Ames, 1994) and confirmed that they acquired γ-H2AX foci and positive staining for senescence-associated β-galactosidase (SA-β-Gal) activity (Fig. S1 G). In this experimental setting, the total level of PGAM protein was greatly reduced, whereas $p21^{CIP1}$ increased as expected (Fig. 1 A). In contrast, the levels of other glycolytic enzymes, including PFK, PGK, enolase, and GAPDH, remained relatively constant (Fig. 1 A). As *PGAM1* and *PGAM2* mRNA levels also remained constant under these conditions (Fig. S1 H), the data suggested that PGAM protein levels might be regulated by proteolysis during SIS. In line with this idea, addition of the proteasome inhibitor MG132 restored the PGAM protein levels in stressed cells (Fig. 1 B). Similar results were obtained in MEFs undergoing Ras-G12V–induced senescence (Fig. 1 C). Stress-induced down-regulation of PGAM protein was also observed in human primary fibroblasts (WI-38, TIG3, and IMR90), but not in cancer cell lines (HeLa, 293T, and SW620) that evade SIS (Fig. S1, I and J).

We previously reported that the PGAM protein can be ubiquitinated (Kondoh et al., 2005), and, consistent with the MG132-sensitive turnover of endogenous PGAM during SIS, a His-tagged ubiquitin purification assay revealed heavy ubiquitination of FLAG-tagged PGAM1 and PGAM2 in primary MEFs exposed to etoposide (Fig. S1, K and L, left) or Ras-G12V (Fig. S1, K and L, right). Ubiquitination of endogenous PGAM could also be observed in these circumstances by immunoprecipitating PGAM and immunoblotting for ubiquitin (Fig. 1 D). Consistently, PGAM enzymatic activity, glycolytic flux, and lactate production were also substantially reduced in the cells exposed to etoposide (Fig. 1 E and Fig. S1 M) or RasG12V (Fig. 1 F and Fig. S1 N). Collectively, our data suggest that PGAM protein is subject to ubiquitin-mediated degradation during SIS.

Pak1 phosphorylates PGAM during SIS and provokes premature senescence in primary fibroblasts

As ubiquitination often requires prior modification of the target protein (Hagai et al., 2012), we investigated whether PGAM might be phosphorylated during SIS, specifically by Pak1. It was previously reported that Pak1 physically interacts with and phosphorylates PGAM in immortalized 293T cells, but that PGAM protein levels are not affected by Pak1 activation (Shalom-Barak and Knaus, 2002). However, in contrast to the situation in 293T cells, we found that Pak1 expression in normal WI-38 human fibroblasts caused a substantial reduction in PGAM protein levels (Fig. 2 A). A similar effect was seen in primary MEFs but only with wild-type Pak1 and not with a version in which the kinase domain was mutated (Fig. 2 B).

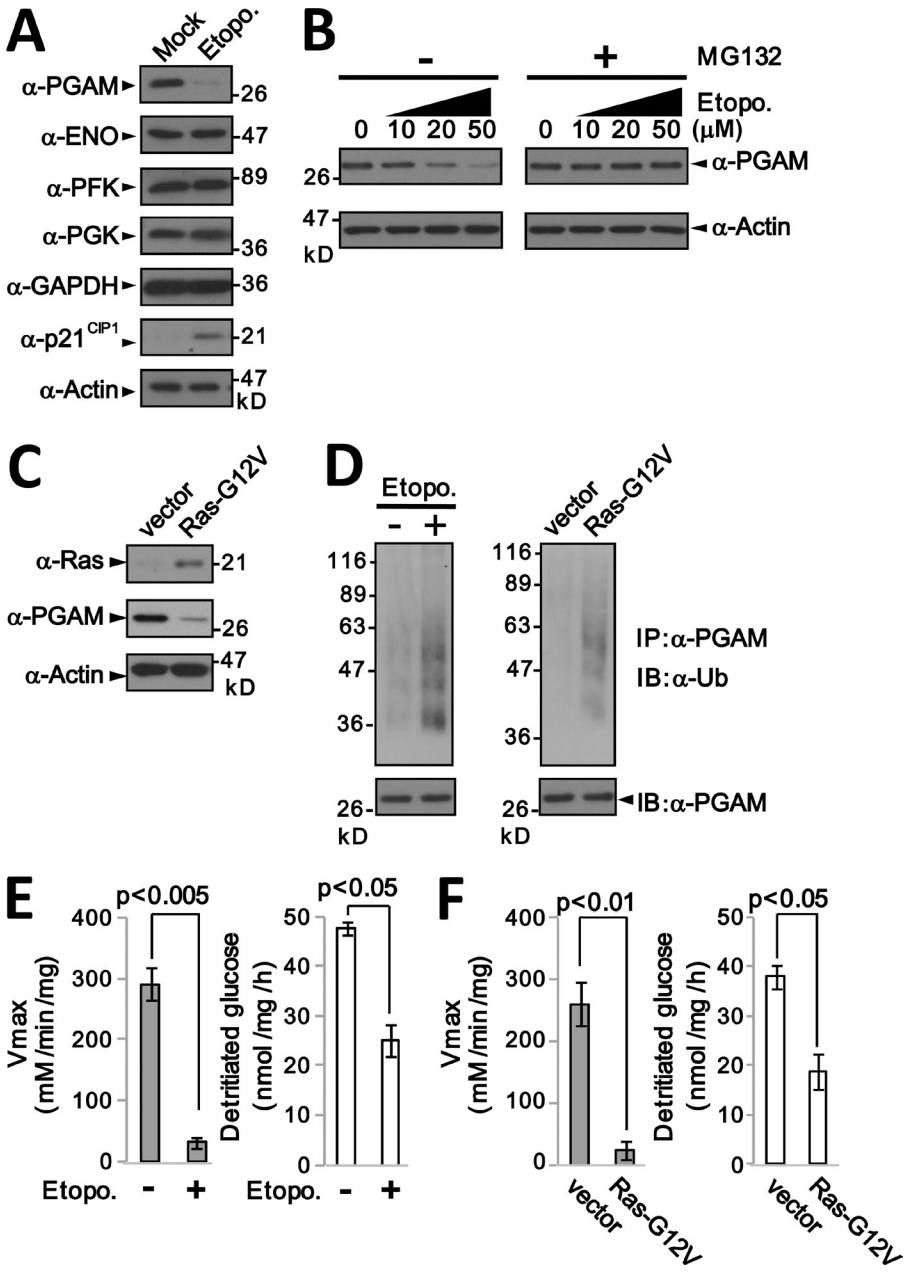

Figure 1. **Down-regulation of PGAM in primary fibroblasts after DNA damage or Ras-G12V expression.** (A) Extracts from primary MEFs (passage 2) treated without (Mock) or with 20 μM etoposide for 6 h were immunoblotted for the indicated proteins. PGAM, phosphoglycerate mutase; ENO, enolase; PFK, phosphofructokinase; PGK, phosphoglycerate kinase; GAPDH, glyceraldehyde 3-phosphate dehydrogenase. Actin was used as a loading control. (B) Proteasome-dependent down-regulation of PGAM protein after DNA damage. Extracts from primary MEFs treated for 6 h with increasing concentrations of etoposide (as indicated) in the presence or absence of the proteasome inhibitor MG132 (20 μM) were analyzed as in A. (C) Immunoblotting for Ras and PGAM in MEFs infected with Ras-G12V or empty vector. (D) Ubiquitination of endogenous PGAM in MEFs exposed to DNA damage (left) or to oncogenic Ras (right). Cell extracts were immunoprecipitated with anti-PGAM antibody and immunoblotted with a monoclonal anti-ubiquitin antibody. (E and F) Measurement of total cellular PGAM activity (left) and glycolytic flux (right) in primary MEFs exposed to DNA damage (E) or expressing Ras-G12V (F). Error bars indicate SEM (n = 3).

Importantly, the effects on PGAM protein levels were reflected in reduced PGAM activity, glycolytic flux, and lactate production (Fig. 2 B).

Concomitant with reduced PGAM activity, ectopic expression of Pak1 provoked features of senescence, including premature cessation of cell proliferation (Fig. 2 C), flattened and enlarged cell morphology, a single large nucleolus, and SA-β-Gal staining (Fig. 2 D). Importantly, the levels of Pak1 protein and mRNA were elevated during SIS resulting from DNA damage (Fig. 2 E and Fig. S2 A).

Previous work identified serines Ser23 and Ser118 as the residues in PGAM1 phosphorylated by Pak1 (Shalom-Barak and Knaus, 2002). As Ser118, but not Ser23, is conserved between PGAM1 and PGAM2, we raised a phospho-specific antibody against a 12–amino acid phosphopeptide centered on Ser118 (Fig. S2 B). Enhanced phosphorylation of Ser118 in PGAM was observed in primary MEFs after treatment with etoposide or expression of Ras-G12V in the presence of MG132 (Fig. 2 E and Fig. S2 C). To confirm that Ser118 is a direct target for Pak1 kinase, we prepared recombinant wild-type (PGAM2-WT) or mutant (PGAM-S118C) PGAM2 proteins and deployed them as substrates in an in vitro kinase assay using Pak1 immunopurified from primary MEFs. The ability of Pak1 to phosphorylate wild-type PGAM2 was increased after exposure of the cells to etoposide (Fig. 2 F). An equivalent increase was not observed using PGAM-S118C as a substrate, which suggests that stress-induced Pak1 mediates phosphorylation of PGAM at S118 (Fig. 2 F).

These data raised the possibility that phosphorylation of PGAM by Pak1 could promote the ubiquitination-mediated degradation of PGAM during SIS. In support of this notion, PGAM protein levels in Pak1-expressing primary MEFs were restored

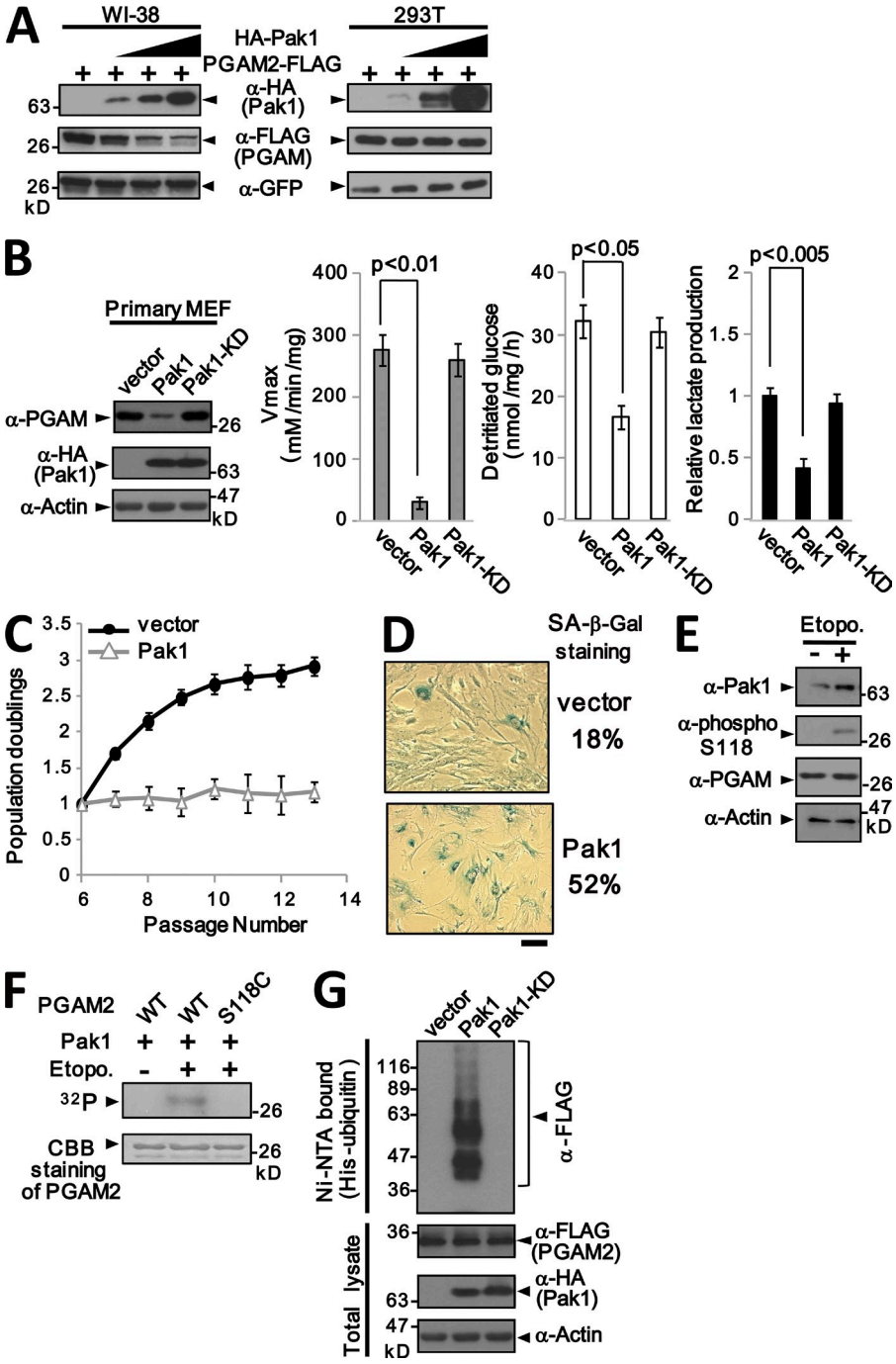

Figure 2. **Pak1 induces down-regulation of PGAM and premature senescence.** (A) Human primary fibroblasts (WI-38, left) or immortalized cells (293T, right) were cotransfected with plasmids encoding GFP, PGAM2-FLAG, and increasing amounts of a plasmid encoding HA-Pak1. Cell lysates were analyzed by SDS-PAGE and immunoblotted for the indicated proteins. (B) Primary MEFs were infected with vectors encoding HA-Pak1 or HA-Pak1-KD, in which kinase activity is inactivated by the K299R mutation. At passage 8, cell extracts were assessed for total PGAM protein levels (far left), PGAM enzymatic activity (second from the left), glycolytic flux (third from the left), and lactate production (far right). (C) Growth curves of primary MEFs infected with Pak1 or empty vector, passaged in a 3T3 protocol. (D) Example of SA-β-Gal staining in Pak1-expressing and control MEFs. Bar, 20 µm. (E) Primary MEFs at early passages were treated with 20 µM etoposide in the presence of 20 µM MG132, and cell lysates were immunoblotted with antibodies against Pak1 and phospho-Ser118 in PGAM as indicated. (F) Pak1 kinase phosphorylates PGAM2 at Ser118 in vitro. Pak1 proteins were immunoprecipitated from primary MEFs treated with 20 µM etoposide, as indicated. The precipitated proteins were co-incubated for 30 min with recombinant PGAM2 or the S118C mutant, and the incorporation of ^{32}P was detected by autoradiography. (G) Pak1 promotes ubiquitination of PGAM2. MEFs were transfected with PGAM2-FLAG, His_6-ubiquitin, and either HA-Pak1 or HA-Pak1-KD. Ubiquitinated proteins were recovered using Ni-NTA agarose and immunoblotted with FLAG antibody. In B and C, error bars indicate SEM (n = 3).

after MG132 treatment (Fig. S2 D), and polyubiquitinated forms of PGAM were detected in Pak1-expressing MEFs (Fig. 2 G and Fig. S2, E and F).

Phosphorylation by Pak1 is required for ubiquitination and degradation of PGAM

Next we examined whether phosphorylation by Pak1 is required for the degradation of PGAM, taking three different approaches. First, we used two different shRNAs against mouse Pak1 to knock down the level of endogenous Pak1 in primary MEFs, as assessed by real-time qRT-PCR and Western blotting (Fig. 3 A). Importantly, after ablation of Pak1, the level of endogenous PGAM protein was increased ∼1.7–1.9-fold compared with that in control cells (Fig. 3 A). Also, the appearance of ubiquitinated forms of PGAM after DNA damage was reduced in Pak1-deficient MEFs (Fig. 3 B).

Second, we asked whether mutation of the Pak1 phosphorylation sites on PGAM restores its stability. Nonphosphorylatable mutants of PGAM2 in which Ser118 was changed to either Cys or Ala (PGAM2-S118C and PGAM2-S118A) were generated by site-directed PCR mutagenesis. Cotransfection experiments in MEFs revealed that the level of wild-type PGAM, but not of PGAM2-S118C or PGAM2-S118A, was reduced in parallel to the increase of Pak1 expression (Fig. 3 C and Fig. S2 G). We determined the stability of the PGAM2-FLAG protein in primary MEFs by blocking protein synthesis

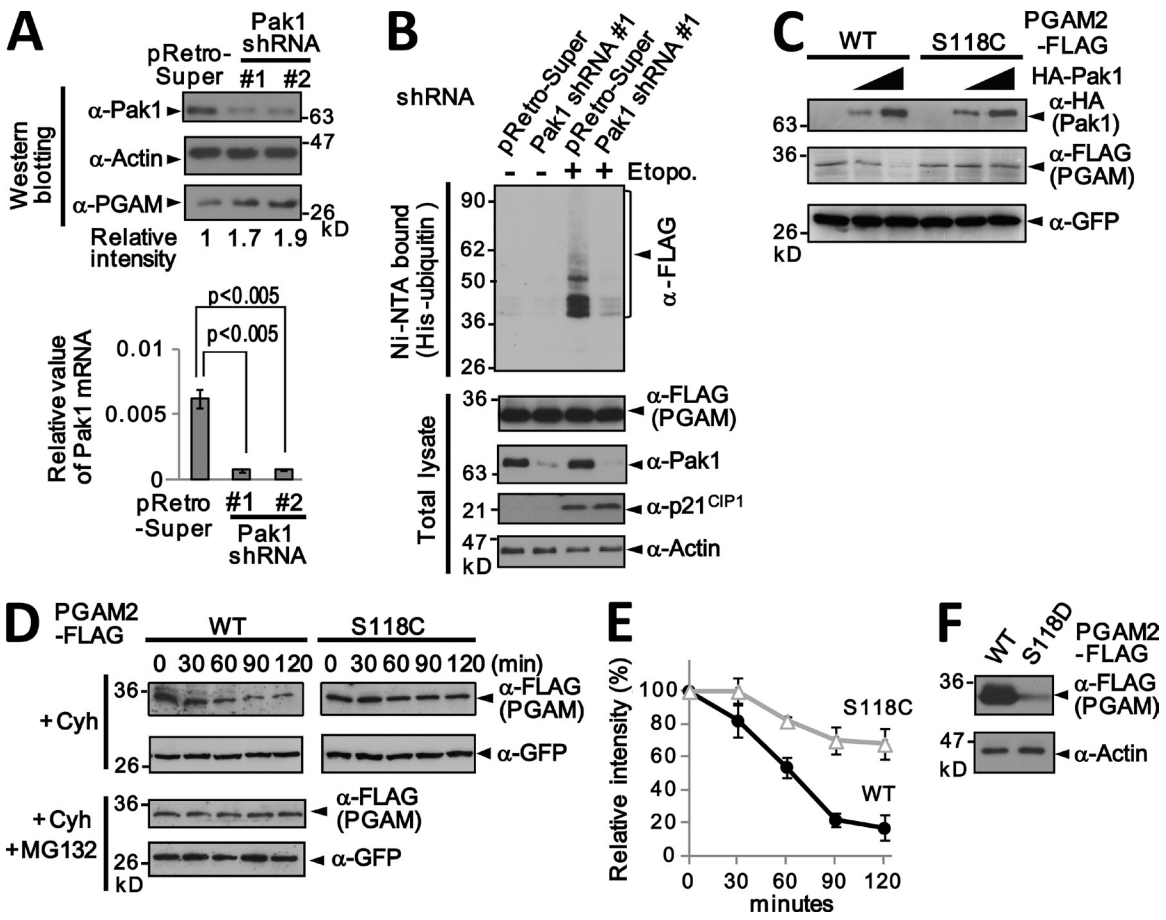

Figure 3. **Pak1-mediated phosphorylation of PGAM on serine 118 dictates PGAM turnover.** (A) Primary MEFs were infected with a retrovirus encoding shRNA against Pak1 (Pak1 shRNA Nos. 1 and 2) or vector control, and the effects on Pak1 mRNA and protein levels were determined by real-time qRT-PCR (bottom) or by immunoblotting (top). The levels of Pak1 mRNA were presented as relative values after normalization by those of RPL13. Probing the same samples with an anti-PGAM antibody showed that Pak1 knockdown by Pak1 shRNA Nos. 1 and 2 caused an ~1.7 and 1.9-fold increase in PGAM levels, respectively. (B) Pak1 knockdown impairs ubiquitination of PGAM2 in stressed cells. MEFs expressing PGAM2-FLAG and His_6-ubiquitin were infected with Pak1 shRNA or vector control, and the cells were then treated with or without 20 µM etoposide. Ubiquitinated proteins were recovered using Ni-NTA agarose and immunoblotted with FLAG antibody. (C) MEFs were cotransfected with plasmids encoding GFP, either the WT or S118C variant of PGAM2-FLAG, and increasing amounts of a plasmid encoding HA-Pak1. Cell extracts were analyzed by SDS-PAGE and immunoblotted with the indicated antibodies. (D) Primary MEFs infected with retroviral plasmids encoding GFP and either PGAM2-WT-FLAG or PGAM2-S118C-FLAG were treated with cycloheximide, and samples taken at the indicated times were immunoblotted for PGAM2-FLAG and GFP. (E) The data in D were used to plot the relative band intensity of PGAM2-FLAG at different time points normalized to that of GFP. (F) Primary MEFs were infected with retroviral vectors encoding PGAM2-WT-FLAG or PGAM2-S118D-FLAG and cultured under normal conditions. Whole cell extracts were analyzed by SDS-PAGE and immunoblotted with antibodies against FLAG and actin. In A and E, error bars indicate SEM (n = 3).

with cycloheximide. The level of PGAM2-WT-FLAG rapidly decreased after cycloheximide treatment (Fig. 3 D, top left), but was restored by treatment with proteasome inhibitor (Fig. 3 D, bottom left). The S118C mutation restored PGAM2 stability by about twofold compared with that of the WT protein (Fig. 3, D and E).

Third, we changed the Ser118 residue to aspartic acid (PGAM-S118D) to mimic the phosphorylated form of PGAM, and examined the effects on stability. In transfected MEFs, under normal culture conditions, the expression of PGAM2-S118D-FLAG was much lower than that of PGAM2-WT-FLAG (Fig. 3 F). In this setting, we also noted that PGAM2-S118D-FLAG, but not PGAM2-S118A-FLAG, was highly ubiquitinated (Fig. S2 H). Collectively, our data indicate that Pak1-dependent phosphorylation of PGAM on Ser118 promotes its ubiquitin-dependent proteasomal degradation.

Mdm2 mediates PGAM ubiquitination

As ubiquitination generally requires a substrate-specific ubiquitin ligase (Hershko and Ciechanover, 1998), we next sought to identify the E3 ubiquitin ligase that targets PGAM. Having shown that PGAM is vulnerable to ubiquitin-mediated turnover in primary fibroblasts but not in 293T cells (Fig. 2 A), we extended these analyses to include additional examples of immortalized cells in order to uncover potentially relevant oncogenic determinants. Using a panel of colon cancer cell lines, we found that PGAM ubiquitination was induced by DNA damage in cells with wild-type p53 (HCT116 and RKO) but not in those with impaired p53 function (HT29 and Sw620; Fig. S3 A; Rodrigues et al., 1990). Consistent with the possibility that ubiquitination of PGAM might be p53 dependent, endogenous PGAM levels were down-regulated after tetracycline-induced expression of p53-GFP fusion protein in the TGP53-4 mouse cell line (Fig. S3 B,

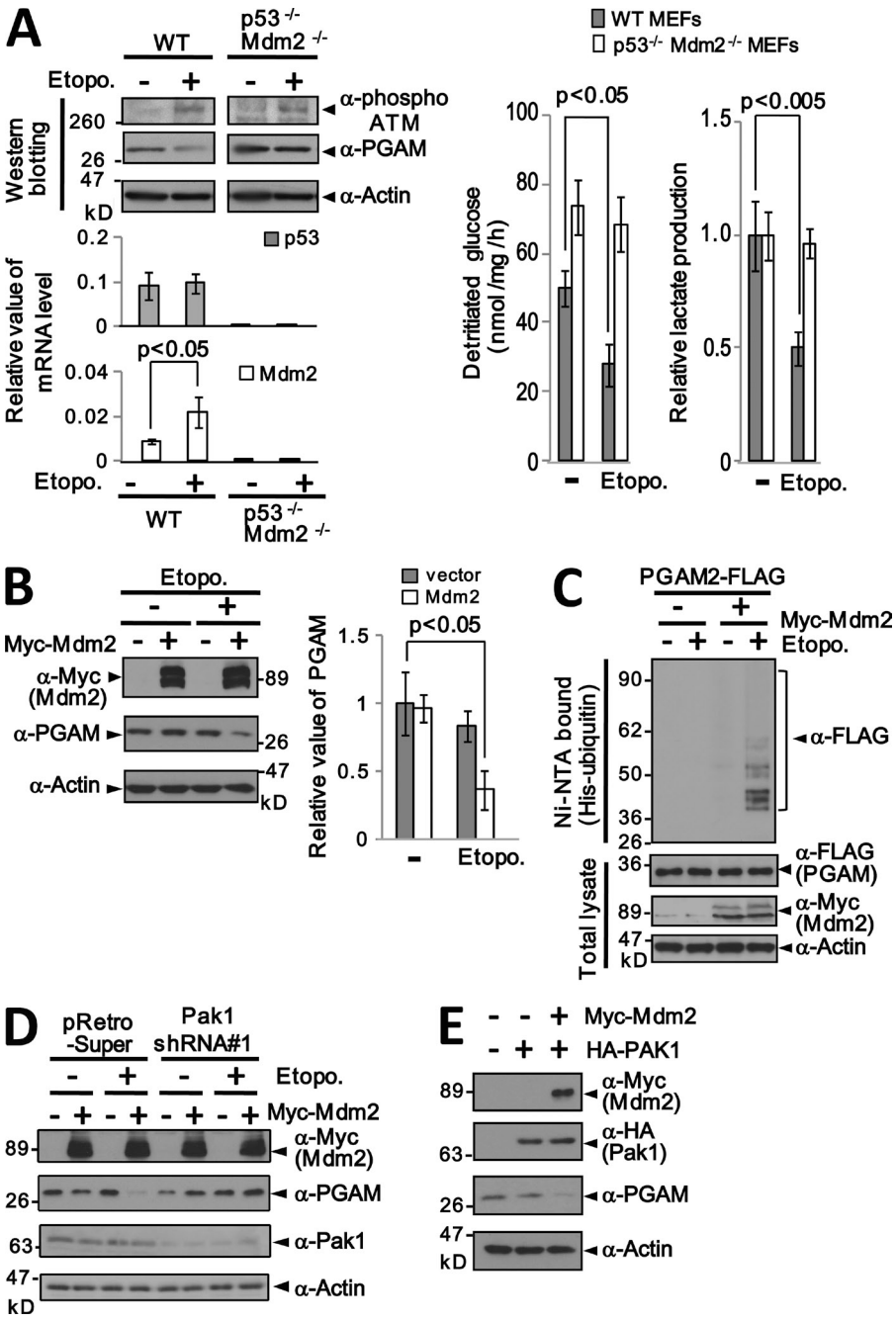

Figure 4. **Role of Mdm2 in PGAM ubiquitination.** (A) Effects of DNA damage (20 µM etoposide) on PGAM protein and RNA levels in wild-type and $p53^{-/-}Mdm2^{-/-}$ MEFs (left). The top panels show the results of immunoblotting; the bottom panels show real-time qRT-PCR for the indicated target genes. The levels were presented as relative values after normalization by those of RPL13. The effect of DNA damage on glycolytic flux (middle) and lactate production (right) in wild-type and $p53^{-/-}Mdm2^{-/-}$ MEFs is shown. (B) $p53^{-/-}Mdm2^{-/-}$ MEFs were transfected with control vector or a vector encoding Myc-Mdm2, and treated with or without etoposide. Extracts were immunoblotted for the indicated proteins (left), and band intensities were used to assess the levels of PGAM relative to those of actin in each sample (right). The results were normalized to the PGAM/actin ratio in untreated cells. (C) Myc-Mdm2 restores DNA-damage dependent ubiquitination of PGAM2-FLAG in $p53^{-/-}Mdm2^{-/-}$ MEFs. (D) Pak1 knockdown impairs Mdm2-mediated turnover of PGAM after DNA damage. $p53^{-/-}Mdm2^{-/-}$ MEFs infected with Pak1 shRNA or control retroviruses were transfected with Myc-Mdm2 and treated with etoposide as indicated. Cell extracts were analyzed by SDS-PAGE, and endogenous PGAM was detected by immunoblotting. (E) Assessment of endogenous PGAM protein levels in $p53^{-/-}Mdm2^{-/-}$ MEFs expressing HA-Pak1 and Myc-Mdm2 as indicated. In A and B, error bars indicate SEM ($n = 3$).

left), accompanied by a decline in glycolytic flux and lactate production (Fig. S3 B, middle and right). Conversely, the ability of Ras-G12V to induce down-regulation of PGAM in MEFs was abrogated by coexpression of HPV E6, which facilitates p53 degradation (Fig. S3 C).

As these data indicate that PGAM is ubiquitinated in a p53-dependent manner, we considered Mdm2 as a likely candidate for the relevant ubiquitin ligase. Mdm2 is both a transcriptional target for p53 and responsible for its ubiquitin-mediated degradation (Haupt et al., 1997; Kubbutat et al., 1997; Prives, 1998). Importantly, we did not observe down-regulation of PGAM, glycolytic flux, or lactate production after DNA damage in $p53^{-/-}$ or $p53^{-/-}Mdm2^{-/-}$ double knockout (DKO) MEFs (Fig. 4 A and Fig. S3 D). However, down-regulation and ubiquitination of PGAM1 and PGAM2 was reinstated after ectopic expression of Myc-Mdm2 in DKO MEFs (Fig. 4, B and C; and Fig. S3 E). This effect was Pak1 dependent, as shRNA-mediated knockdown of Pak1 reduced the turnover of PGAM in Myc-Mdm2–expressing DKO MEFs (Fig. 4 D and Fig. S3 F). Moreover, coexpression of Myc-Mdm2 and HA-Pak1 induced PGAM turnover in unstressed DKO MEFs (Fig. 4 E). The S118C or S118A mutation restored PGAM2 stability in DKO MEFs coexpressing Myc-Mdm2 and HA-Pak1 (Fig. S3, G and H). Collectively, the data imply that Mdm2 has a critical role in Pak1-dependent degradation of PGAM.

To investigate whether Mdm2 is directly responsible for ubiquitinating PGAM, we first confirmed that the proteins physically interact in the cell. Myc-Mdm2 can be coimmunoprecipitated

with both PGAM1 and PGAM2 when the proteins are expressed in DKO MEFs (Fig. 5, A and B). To gain further insights, we constructed a series of deletions and point mutations in PGAM2-FLAG (Fig. 5 C, top) and showed that Myc-Mdm2 coprecipitated with full-length PGAM2-FLAG (T1) and with the central one-third of the protein (T4). However, the most robust interaction was with the N-terminally deleted variants of PGAM-FLAG (T2 and TC; Fig. 5 C).

Remarkably, the S118D mutation, which mimics S118 phosphorylation, enhanced the binding of full-length PGAM2 to Mdm2 (Fig. 5 D), which suggests that Pak1-dependent phosphorylation at S118 promotes the interaction. Moreover, DNA damage facilitated the association between endogenous PGAM and Mdm2 in primary MEFs (Fig. 5 E) and also of the ectopically expressed proteins in DKO MEFs (Fig. 5 F). Conversely, shRNA-mediated knockdown of Pak1 abrogated the physical interactions between Myc-Mdm2 and PGAM-FLAG (Fig. 5 G). Based on these results, we concluded that the physical interaction between PGAM and Mdm2 is facilitated by Pak1-dependent phosphorylation after DNA damage.

Mdm2 functions as an E3 ubiquitin ligase for PGAM in vitro

As further confirmation that Mdm2 functions directly as an E3 ubiquitin ligase for PGAM, we reconstituted the reaction in vitro using recombinant proteins. Ubiquitination is accomplished by the coordinated actions of a ubiquitin-activating enzyme (E1), a ubiquitin-conjugating enzyme (E2), and a ubiquitin-ligase (E3). The assays comprised UBE1 as the E1, UbcH5b as the E2 protein, human Mdm2 as the E3 ligase, and PGAM2 as the substrate (Fig. S4 A), and functionality was confirmed using recombinant p53 protein as a control (Fig. 6 A). Although full-length PGAM2 did not appear to be ubiquitinated in vitro as a recombinant protein (Fig. 6 A), the central domain (T4) showed strong evidence for monoubiquitination and some degree of polyubiquitination (Fig. 6 B). Although the N- and C-terminal domains of PGAM2 (TN and TC, respectively) were not modified, polyubiquitination was clearly observed with the T2 construct, which contains both the central and the C-terminal domains of PGAM2 (Fig. 6, C and G), in line with its more avid binding to Mdm2 (Fig. 5 C). Importantly, a catalytically inactive mutant of Mdm2, C464A (Kubbutat et al., 1999), did not ubiquitinate PGAM2-T2 in vitro (Fig. 6 C), which supports the idea that Mdm2 directly ubiquitinates PGAM.

Full-length PGAM2 contains 20 lysine residues in total (Fig. 6 D), seven of which are located in the central domain that appears to be the major target for ubiquitination. Ser118 is also located in this central domain (Fig. S4 B). Mutated versions of PGAM2 were generated in which either four or seven of the lysine residues flanking Ser118 were changed to arginine (PGAM2-4R and -7R; Fig. 6 D and Fig. S4 B). These mutations did not affect the catalytic properties of PGAM2 as judged by its ability to stimulate glycolytic flux and lactate production in primary MEFs (Fig. S4 C). However, immunoblot analyses indicated that the down-regulation of PGAM by Pak1 in primary MEFs was partially alleviated by the 4R mutation, and completely alleviated by the 7R mutation (Fig. S4 D). The 7R mutation also restored PGAM catalytic activity, glycolytic flux, and lactate production in Pak1-expressing MEFs (Fig. S4 E). Strikingly, the 7R mutation rendered PGAM resistant to degradation by DNA damage (Fig. 6 E), and completely inhibited PGAM ubiquitination in cultured cells (Fig. 6 F and Fig. S4 F) and in vitro (Fig. 6 G).

Stabilization of PGAM restores the proliferative potential of primary fibroblasts under stress conditions

Although Mdm2 is generally considered to be an oncogene, its role is subtle, and ectopic expression of wild-type Mdm2 has been reported to cause cell cycle arrest (Brown et al., 1998). Mdm2 contains so-called growth inhibitory domains (ID1 and ID2; Fig. 7 A) that are aberrantly spliced out in some human cancers (Brown et al., 1998). These observations suggest that in some contexts Mdm2 can function as a tumor suppressor (Manfredi, 2010). Interestingly, we noticed that after DNA damage, wild-type MEFs expressing Mdm2 displayed reduced viability compared with control cells (Fig. 7 B). A plausible explanation would be that the negative effects of Mdm2 on cell proliferation and viability reflect destabilization of PGAM. In line with this idea, coexpression of PGAM-7R restored cell viability and PGAM activity in Mdm2-expressing wild-type MEFs (Fig. 7, C and D).

An obvious corollary would be that mutations in Mdm2 that abolish its negative effects on PGAM might be pro-tumorigenic. According to the Catalogue of somatic mutations in cancer (COSMIC) database (http://www.sanger.ac.uk/genetics/CGP/cosmic/), three potentially oncogenic mutations in Mdm2 have been identified: Y281H in glioma and the W329G and M459I mutations in lung carcinoma (Cancer Genome Atlas Research Network, 2008; Ding et al., 2008). Y281H and W329G are located in the ID2 domain, whereas M459I is located in the RING finger motif that is essential for the ubiquitin ligase activity of Mdm2 (Fig. 7 A and Lipkowitz and Weissman, 2011).

We constructed mammalian expression vectors encoding the three cancer-associated variants of Mdm2, as well as an additional mutation in the catalytic RING finger domain (C464A), and evaluated their effects on both PGAM and p53. As Mdm2 can have an impact on p53 function both catalytically, by promoting its ubiquitination, or noncatalytically, by blocking its transcriptional activation domain (Kubbutat et al., 1999; Poyurovsky et al., 2003), we first assessed whether the variant forms of Mdm2 could suppress p53 activity in promoter assays. In the experiment, all four of the Mdm2 variants suppressed p53 activity on the $p21^{CIP1}$, Bax, and Mdm2 promoters to a degree similar to wild-type Mdm2 (Fig. S5 A). In contrast, only the mutations in RING domain (M459I and C464A) abolished the ability of Mdm2 to ubiquitinate p53 in cells and in vitro (Fig. 6 A and Fig. S5, B–D). Importantly, when assessed for their effects on PGAM2 stability, in conditions of DNA damage, all of the Mdm2 variants were at least partially impaired, and M459I fully so (Fig. 7, E–G). The impaired ubiquitination of PGAM2 shown by the cancer-associated Mdm2-M459I variant was comparable to that of the Mdm2-C464A mutant (Fig. S5 E). However, the M459I mutation did not abolish the physical interaction between Mdm2 and either PGAM or p53 (Fig. S5, F and G).

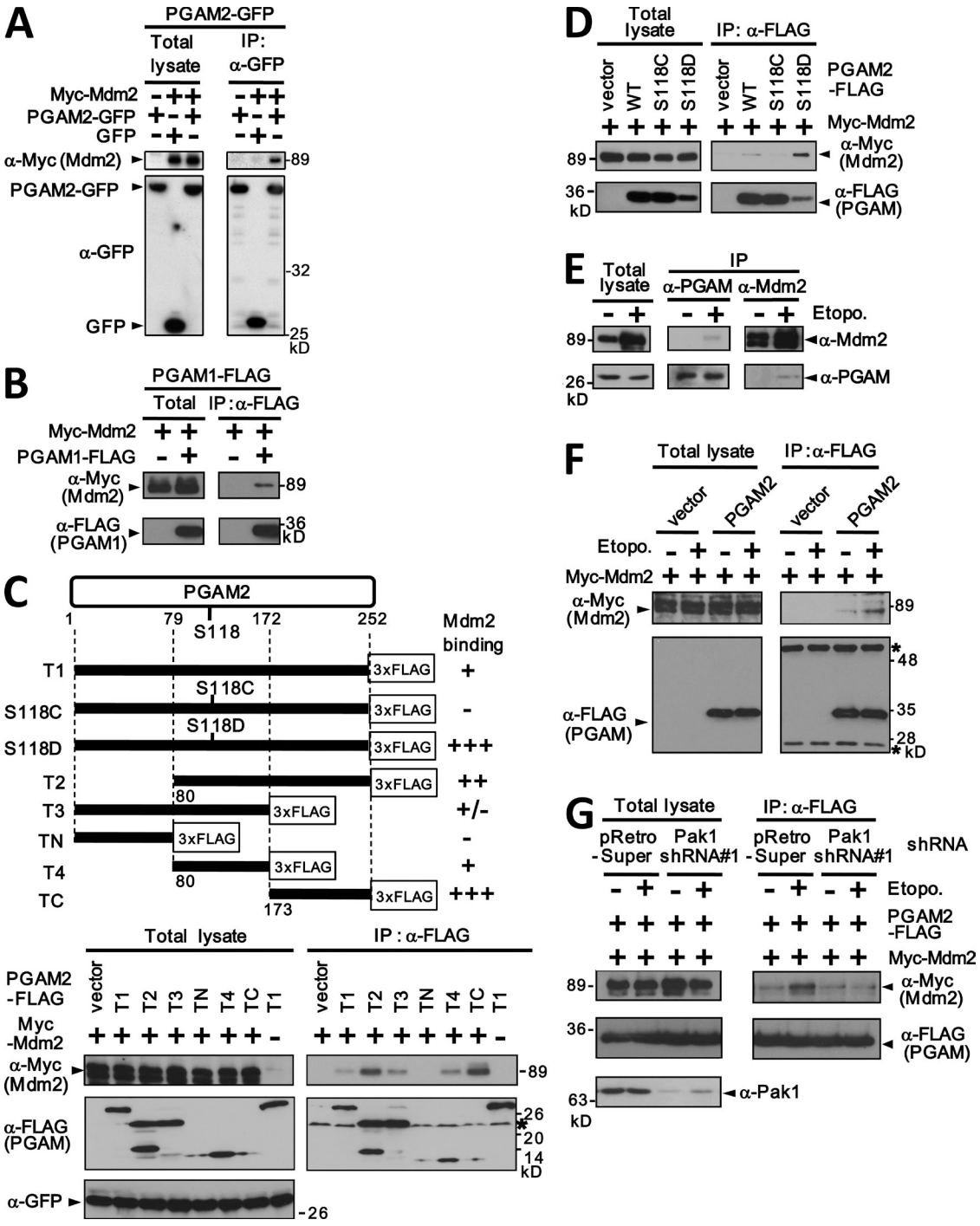

Figure 5. **Pak1-mediated phosphorylation of PGAM2 facilitates its interaction with Mdm2.** (A) *p53*$^{-/-}$*Mdm2*$^{-/-}$ MEFs were transfected with vectors encoding PGAM2-GFP, GFP, and Myc-Mdm2 as indicated. Cell lysates were either analyzed immediately (left) or after immunoprecipitation with an anti-GFP antibody (right), and immunoblotted with antibodies against Myc and GFP. (B) Coimmunoprecipitation of PGAM1-FLAG with Myc-Mdm2. *p53*$^{-/-}$*Mdm2*$^{-/-}$ MEFs were transfected with the indicated vectors and cell lysates were either analyzed directly (left) or after immunoprecipitation with an anti-FLAG antibody (right). (C) Schematic diagram of PGAM2 deletion mutants and the location of serine 118 (top). The relative binding of each mutant to Myc-Mdm2, shown on the right, was assessed by coimmunoprecipitation (bottom). Extracts from *p53*$^{-/-}$*Mdm2*$^{-/-}$ MEFs transfected with the indicated plasmids were immunoprecipitated with anti-FLAG antibody and immunoblotted for Myc, FLAG, and GFP as indicated. Asterisks indicate the heavy and light chains of immunoglobulin. (D) Coimmunoprecipitation of Mdm2 and PGAM2-S118D under normal culture conditions. *p53*$^{-/-}$*Mdm2*$^{-/-}$ MEFs were transfected with Myc-Mdm2 and the indicated PGAM2-FLAG mutants. (E) Reciprocal coimmunoprecipitation of endogenous Mdm2 protein with endogenous PGAM protein. Extracts from primary MEFs, treated with or without etoposide in the presence of 20 µM MG132, were immunoprecipitated with either anti-PGAM or anti-Mdm2 antibodies and immunoblotted with the same reagents. (F) DNA damage facilitates the physical interaction between PGAM and Mdm2. *p53*$^{-/-}$*Mdm2*$^{-/-}$ MEFs expressing Myc-Mdm2 and PGAM2-FLAG were treated with and without 20 µM etoposide, as indicated. Cell lysates were either analyzed immediately (left) or after immunoprecipitation with an anti-FLAG antibody (right). (G) The physical interaction between Mdm2 and PGAM2 is Pak1 dependent. *p53*$^{-/-}$*Mdm2*$^{-/-}$ MEFs were infected with Pak1 shRNA or control virus. The cells were then transfected with PGAM2-FLAG and Myc-Mdm2 and subjected to DNA damage with 20 µM etoposide. Cell extracts were immunoprecipitated with anti-FLAG antibody and immunoblotted for the FLAG and Myc epitopes.

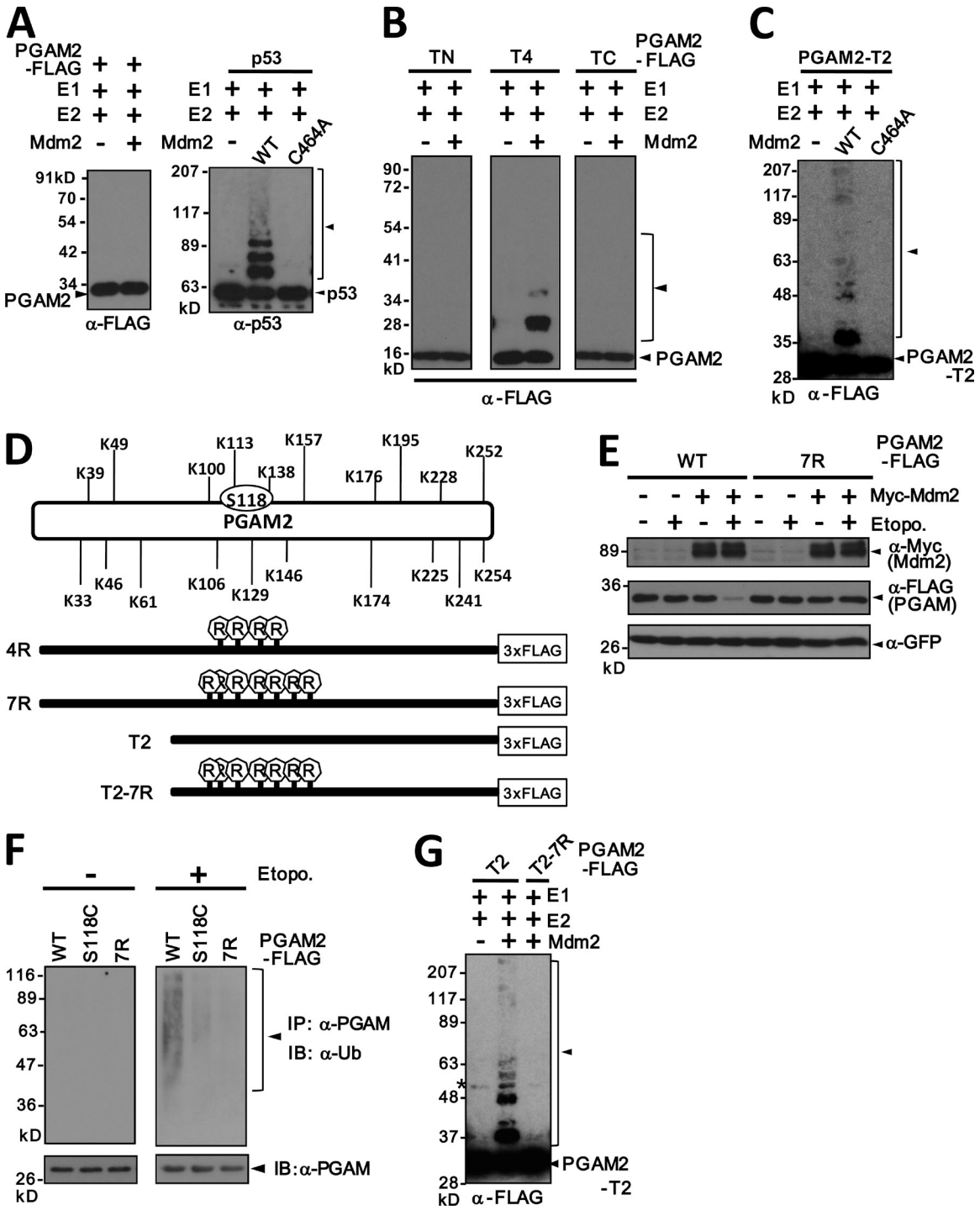

Figure 6. **Mdm2 ubiquitinates PGAM2 in vitro.** (A) An in vitro ubiquitination system comprising recombinant UBE1, UbcH5b-His, Mdm2, and His_6-ubiquitin was tested for its ability to ubiquitinate full-length recombinant PGAM2-FLAG (left) or p53 (right). Mdm2-C464A was used as a negative control. Ubiquitination of p53 resulted in the formation of a ladder of bands. (B) The same assay was performed on the deleted versions of PGAM2 described in Fig. 5 C. Only PGAM2-T4-FLAG, corresponding to residues 80–172 in PGAM2, was efficiently ubiquitinated under these conditions. (C) PGAM2-T2-FLAG is ubiquitinated in vitro by wild-type Mdm2, but not by a catalytically inactive mutant of Mdm2 (Mdm2-C464A). (D) Schematic representation of PGAM2, showing the location of lysine residues relative to Ser118. The 7R-FLAG and 4R-FLAG variants of PGAM2 were generated by site-directed mutagenesis of either seven or four lysine residues in the central domain as indicated. The mutated residues in the 4R mutant were K106, K113, K129, and K138, whereas three additional residues, K100, K146, and K157, were mutated in 7R. PGAM2-T2-7R-FLAG is an N-terminally truncated version of 7R. (E) *p53*$^{-/-}$*Mdm2*$^{-/-}$ MEFs were cotransfected with expression vectors encoding GFP, Myc-Mdm2, and either PGAM2-WT-FLAG or PGAM2-7R-FLAG. After treatment with or without 20 μM etoposide, cell extracts were analyzed by SDS-PAGE and immunoblotting. (F) Mutations in PGAM2 impair its ubiquitination. Primary MEFs expressing the indicated forms of PGAM2-FLAG were treated with or without etoposide, followed by MG132 treatment. Immunoprecipitated PGAM2-FLAG was analyzed by immunoblotting with anti-Ubiquitin antibody (α-Ub; top) and anti-FLAG antibody (bottom). (G) Mdm2 can ubiquitinate PGAM2-T2-FLAG, but not PGAM2-T2-7R-FLAG, in vitro. The indicated recombinant proteins were used in an in vitro ubiquitination assay as in A. The asterisk indicates a nonspecific band. The arrowhead indicates polyubiquitinated proteins.

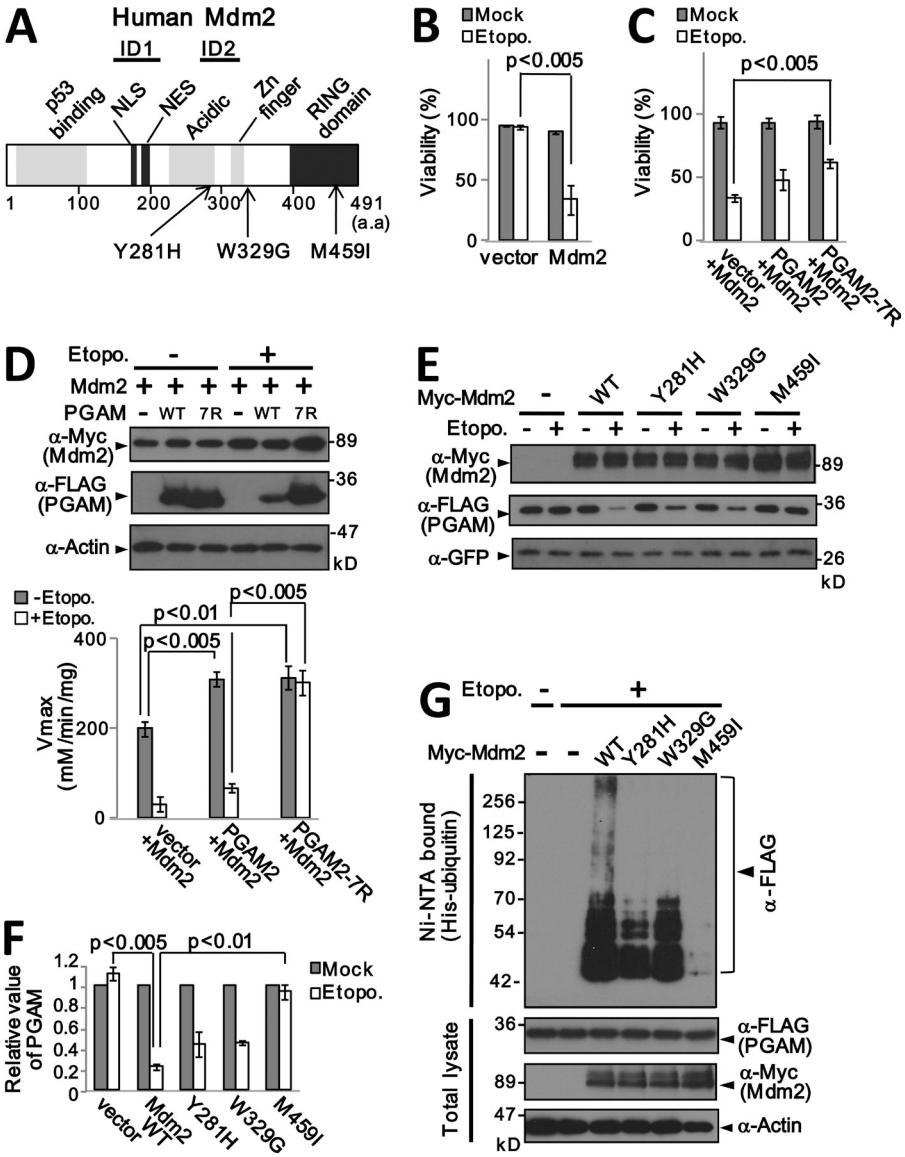

Figure 7. **Stabilization of PGAM by mutation of Mdm2 or PGAM retains cell viability.** (A) Schematic of the reported domain structure of Mdm2 and the location of cancer-associated mutations in human Mdm2 according to the COSMIC database. (B) Ectopic expression of Mdm2 reduces the viability of wild-type MEFs after DNA damage. Viable cells were counted by trypan blue staining. (C) The ability of PGAM2 variants to counteract the effects of Mdm2 and etoposide on cell viability. (D) Primary MEFs infected with vectors encoding Mdm2 and either PGAM2-WT-FLAG or PGAM2-7R-FLAG as indicated were treated with or without etoposide, and the levels of PGAM protein were assessed by immunoblotting (left). Samples of cell extract were also used to measure PGAM enzymatic activity (right). The viability of these cells is shown in C. (E) The ability of Mdm2 variants to restore PGAM2 protein levels after DNA damage. (F) Relative quantitation of the PGAM signal intensity in E normalized to that of GFP. (G) *p53*$^{-/-}$*Mdm2*$^{-/-}$ MEFs were cotransfected with His-ubiquitin, PGAM2-FLAG, and the indicated Mdm2 variants (WT, Y281H, W329G, or M459I). The cells were treated with or without etoposide, and cell extracts were analyzed by immunoblotting, either immediately (bottom) or after recovery of His-tagged ubiquitinated proteins on Ni-NTA agarose under denaturing condition (top). In B, C, D, and F, error bars indicate SEM (n = 3).

Collaboration between PGAM2, Mdm2, and Ras-G12V in cell transformation

Interestingly, the Y281H and M459I mutations in Mdm2, in glioma and lung carcinoma, respectively, were accompanied by activating mutations in the G12 residue of Ras (G12D and G12C). We therefore explored whether Ras-G12V and Mdm2 had cooperative effects on the proliferative potential of primary MEFs. Neither wild-type Mdm2 nor any of the three mutants (Y281H, W329G, and M459I) were able to immortalize Ras-G12V–expressing wild-type MEFs, whereas ablation of p53 with HPV E6 readily enabled the cells to bypass Ras-induced senescence (Fig. 8 A and Fig. S5 H). However, we obtained a strikingly different answer when these assays were performed using cells derived from a transgenic mouse line that we have developed, in which PGAM2-FLAG expression is driven by the *CAG* promoter (Niwa et al., 1991), a fusion between the cytomegalovirus immediate-to-early enhancer element and chicken *β-actin* promoters (Fig. 8 B). MEFs from the *PGAM*-Tg mice displayed enhanced glycolytic flux and lactate production (Fig. S5 I). When we infected the cells with Ras-G12V and the relevant mutants of Mdm2 (WT, Y281H, W329G, and M459I), and passaged them in a 3T3 protocol, the MEFs expressing Ras-G12V and Mdm2-M459I appeared to be immortal and were able to grow as anchorage-independent colonies in soft agar (Fig. 8, A, C, and D). The Mdm2 variants were expressed at equivalent levels shown by Western blotting (Fig. S5 J). Ubiquitination of PGAM protein was barely detectable in the *Ras-G12V/Mdm2-M459I/PGAM*-Tg MEFs, compared with the controls or cells transduced with the other Mdm2 mutants (Fig. 8 E and Fig. S5 K). Moreover, in the *Ras-G12V/Mdm2-M459I/PGAM*-Tg MEFs, both glycolytic flux and lactate production were up-regulated (Fig. 8 F and Fig. S5 L).

We previously reported that MEFs expressing PGAM2 and Ras-G12V were unable to grow in soft agar (Kondoh et al., 2005), and, consistent with this observation, we found that Ras-G12V–expressing *PGAM2*-Tg MEFs could not form tumors in nude mice (Fig. 8 G). Of the cells expressing different Mdm2 variants, only the *Ras-G12V/Mdm2-M459I/PGAM*-Tg MEFs formed tumors in nude mice at a significant frequency (Fig. 8, G and H and Table 1). We presume that the M459I RING finger

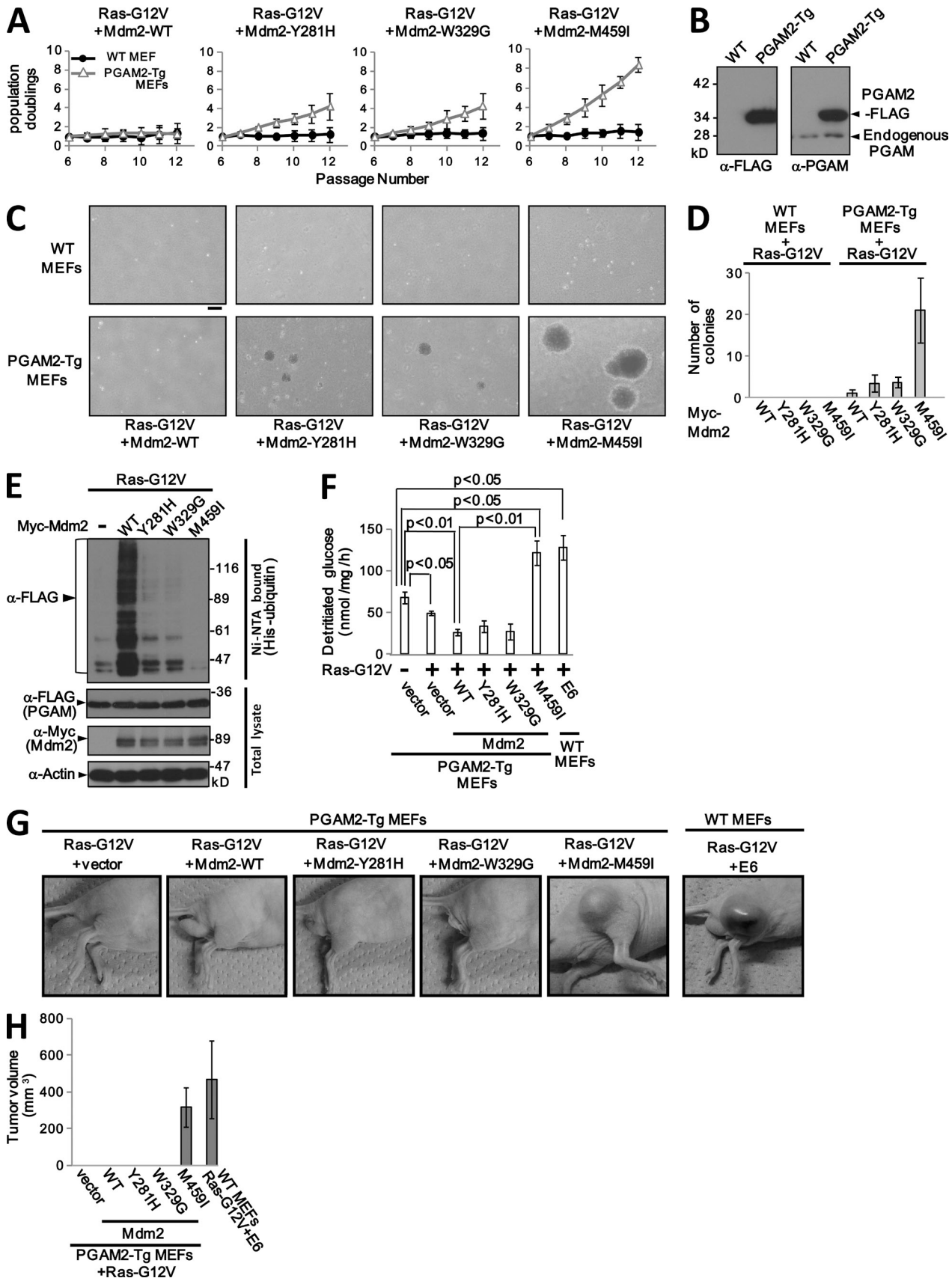

Figure 8. **Collaboration between PGAM2, Mdm2 and RasG12V in cell transformation.** (A) The ability of the indicated Mdm2 mutants to bypass RasG12V–induced senescence in *PGAM2*-Tg but not wild-type MEFs. (B) Relative levels of endogenous and FLAG-tagged PGAM2 in primary MEFs isolated from either wild-type or transgenic C57BL/6 mice that overexpress PGAM2-FLAG from the *CAG* promoter. Whole cell extracts of MEFs were analyzed

Table 1. **Formation of subcutaneous tumors in nude mice by PGAM2-Tg MEFs infected with Ras-G12V and various Mdm2 mutants**

Cells	Number tumors/number injected
PGAM2-Tg MEFs/*Ras-G12V* + vector	0/6
PGAM2-Tg MEFs/*Ras-G12V* + *Mdm2-WT*	0/12
PGAM2-Tg MEFs/*Ras-G12V* + *Mdm2-Y281H*	0/6
PGAM2-Tg MEFs/*Ras-G12V* + *Mdm2-W329G*	0/6
PGAM2-Tg MEFs/*Ras-G12V* + *Mdm2-M459I*	5/8
Wild-type MEFs/*Ras-G12V* + *E6*	6/6

Formation of subcutaneous tumors in nude mice after injection of *PGAM2*-Tg MEFs infected with the indicated expression vectors. For each injection, 5×10^6 cells were injected in a volume of 100 µl. Mice were sacrificed after 3 wk of monitoring. Representative results of two independent experiments are shown ($n = 2$).

mutation renders Mdm2 uniquely able to suppress p53 transactivation without destabilizing PGAM under stress conditions. Thus, in the context of activated Ras-G12V, our data imply that both Mdm2 and the glycolytic enzyme PGAM promote neoplastic transformation (Fig. 9).

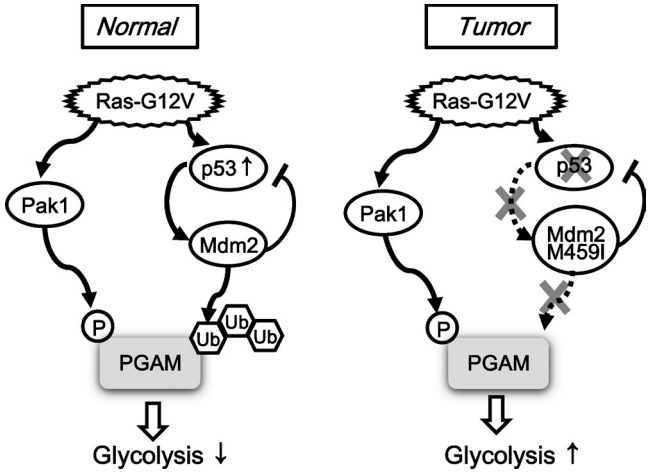

Figure 9. **Model.** Model for PGAM stabilization and effects on glycolysis in different cellular contexts. (left) In normal cells, Ras-G12V expression triggers PGAM ubiquitination associated with a decline of glycolysis via Pak1/Mdm2 activation. (right) The situation in tumors induced by Ras-G12V and Mdm2-M459I associated with stabilization of PGAM and enhanced glycolysis. Note that according to the International Cancer Genome Consortium (2010), missense mutations in Mdm2 are relatively rare, and only 2 of the 24 variants recorded thus far affect the RING domain.

Discussion

With the notable exception of PGAM, most glycolytic enzymes are transcriptionally regulated by HIF-1α (Iyer et al., 1998) or c-Myc (Osthus et al., 2000). Here we show that under conditions of DNA damage or oncogenic signaling, each of which provokes premature senescence in primary cells, PGAM is posttranscriptionally regulated through phosphorylation-dependent ubiquitination. Turnover of PGAM could account for the marked reduction of glycolytic flux observed in senescent cells, and the mechanistic insights we provide suggest a key role for the p53–Mdm2 axis in these events.

The first step in this process is the activation of Pak1 kinase, a direct downstream effector of Cdc42/Rac1 that is involved in many cellular processes, including cell motility, actin reorganization, gene transcription, and apoptosis, as well as in cancer (Molli et al., 2009). Amplification of the *Pak1* gene has been observed in human tumors (Schraml et al., 2003), whereas ectopic expression of Pak1 promotes hyperplasia in vivo (Wang et al., 2002) and cellular transformation in vitro (Vadlamudi et al., 2000). Moreover, mice that lack Merlin, an inhibitor of Pak1, display a cancer-prone phenotype that is exacerbated by p53 mutation (McClatchey et al., 1998). Here we reveal an unexpected role for Pak1 in cellular senescence in primary MEFs and human dermal fibroblasts exposed to various forms of stress. In this respect, the double-edged sword properties of Pak1 are reminiscent of those of oncogenic Ras-G12V, which elicits senescence in primary cells but cell proliferation and transformation in cells that evade senescence (Serrano et al., 1997).

Our findings also connect Pak1 to the regulation of glycolysis, as its involvement in senescence can be largely explained by its ability to phosphorylate PGAM on Ser118. We present several lines of evidence that in primary cells this event is critical for the subsequent ubiquitination and proteasome-mediated turnover of PGAM. PGAM is stabilized by shRNA-mediated depletion of Pak1 and by mutations that exclude phosphorylation by Pak1, whereas the corresponding phosphomimetic mutation promotes ubiquitination and turnover of PGAM.

Although we cannot discount the possibility that other ubiquitin E3 ligases might target PGAM, Mdm2 emerged as an obvious candidate based on the differential behavior of PGAM in p53-positive and -negative cells. We confirmed that phosphorylation of PGAM by Pak1 promotes the interaction between Mdm2 and PGAM under stress conditions, and that Mdm2 ubiquitinates PGAM in cultured cells and in vitro. The in vitro assays identified seven lysine residues in PGAM that are targets for Mdm2-mediated ubiquitination. Consistent with recent reports that ubiquitination sites are generally close to the preceding phosphorylation event (Hagai et al., 2012), the relevant lysine

by immunoblotting with anti-FLAG or -PGAM antibody. (C) Coexpression of the Mdm2-M459I mutant and Ras-G12V conferred anchorage-independent growth in *PGAM2*-Tg MEFs. Bar, 200 µm. (D) Anchorage-independent colonies in Fig. 8 C were counted after 3 wk. (E) The ability of the indicated Mdm2 variants to promote ubiquitination of PGAM2 in *PGAM2*-Tg/*Ras-G12V* MEFs. (F) Measurement of glycolytic flux in primary *PGAM2*-Tg MEFs expressing the indicated combinations of Ras-G12V and Mdm2 variants (WT, Y281H, W329G, or M459I). Wild-type MEFs expressing HPVE6 were used as a control. (G) *PGAM*-Tg MEFs (5×10^6 cells) expressing Ras-G12V and various mutants of Mdm2 (WT, Y281H, W329G, or M459I) were injected subcutaneously in nude mice, and tumor growth was monitored for 3 wk. Wild-type MEFs expressing Ras-G12V and E6 were used as a positive control. Representative photographs of mice in Table 1 are shown. In A, D, and F, error bars indicate SEM ($n = 3$). (H) Measurement of tumor volumes, which were shown in Table 1. Error bars indicate SEM.

residues in PGAM are located in the central domain, adjacent to the Pak1-phosphorylation site Ser118.

Mdm2 is known to ubiquitinate several other substrates, including the p53 tumor suppressor (Manfredi, 2010), and is therefore viewed as an oncogene. In line with this idea, amplification of the *Mdm2* gene has been observed in several human cancers (Leach et al., 1993; Reifenberger et al., 1993). It was also reported that the combination of Mdm2, oncogenic Ras-G12V, and adenovirus E1A will efficiently transform human primary fibroblasts (Seger et al., 2002). In contrast, we and others have noted that in primary cells, ectopic expression of wild-type Mdm2 induces cell cycle arrest (Brown et al., 1998) or apoptosis under conditions of stress (this paper). Moreover, whereas p53 ablation can rescue MEFs from Ras-G12V-induced senescence, ectopic expression of wild-type Mdm2 cannot.

The differential effects of cancer-associated Mdm2 mutants reveal a plausible explanation. Two of the mutations, Y281H and W329G, in the inhibitory domain 2 (ID2) of Mdm2 partly abolish its ability to ubiquitinate PGAM but not p53. The third mutation, M459I in the RING finger domain, completely abolishes ubiquitin ligase activity both for p53 and PGAM, while remaining able to block p53 transactivation. The relative potency of the Mdm2 mutants in PGAM ubiquitination closely correlated with their abilities to rescue PGAM-Tg MEFs from Ras-induced senescence. Strikingly, the combination of the M459I mutant of Mdm2 and oncogenic Ras-G12V was sufficient to transform primary MEFs from PGAM-Tg mice, but not those from wild-type mice. We suspect that this reflects the higher basal levels of glycolysis and lactate production in the PGAM-Tg, which would facilitate the bypassing of senescence. Collectively, the data suggest that in some contexts, Mdm2 might protect cells from transformation by promoting the ubiquitin-mediated turnover of PGAM. Alternatively, up-regulation of PGAM could promote the oncogenic effects of the mutant forms of Mdm2. Consistent with these ideas, the ubiquitination activity of Mdm2 is reported to be differentially regulated in a cellular context– and developmental stage–dependent manner (Itahana et al., 2007; Terzian et al., 2008).

Both enhanced glycolysis (the Warburg effect) and cellular immortalization are recognized as hallmarks of cancerous tissues and cells. Our data on the ubiquitination of PGAM by the p53/Mdm2 axis during SIS might partly explain how these hallmarks are coupled. The activation of p53 during senescence, whether via DNA damage or direct oncogenic signaling, would potentially down-regulate glycolytic flux by promoting Mdm2-mediated turnover of PGAM. Similar effects on glycolysis would be achieved via the transcriptional activity of p53 on other target genes, such as TIGAR and Glut3 (Bensaad et al., 2006; Kawauchi et al., 2008). Thus, p53 might function as a metabolic checkpoint against tumorigenesis partly by modulating the glycolytic pathway (Jones et al., 2005). As we have previously argued (Kondoh et al., 2005), the Warburg effect could represent a metabolic adaptation that enables incipient cancer cells to evade senescence.

Several recent studies have emphasized the importance of PGAM as a therapeutic target for cancer management (Durany et al., 1997, 2000, Evans et al., 2005; Vander Heiden et al., 2010; Hitosugi et al., 2012). Our identification of physiological modulators of PGAM stability might open up new avenues for therapeutic intervention.

Materials and methods

Cell culture

Primary MEFs were isolated from 13.5-d postcoitum embryos of C57BL6 mice as described previously (Carnero et al., 2000). The head and blood organs of embryos were removed, and the torso was placed on a 10-cm plate. The embryo was minced with a scalpel and dispersed in 0.1% trypsin (45 min at 37°C). Cells were grown for two population doublings, followed by retroviral infection or transfection of plasmids. Human primary fibroblast (IMR90, WI-38, and TIG3), human immortalized cell lines (HeLa, 293T, HCT116, RKO, HT-29, and SW620), primary MEFs from *p53*$^{-/-}$, *p53*$^{-/-}$*Mdm2*$^{-/-}$, and *PGAM2*-Tg mice were grown in DMEM with 10% FBS. *PGAM2*-Tg is a strain of transgenic C57BL/6 mice that overexpress PGAM2 under the cytomegalovirus immediate-to-early enhancer element and chicken *β-actin* promoter (*CAG*). The GFP-tagged p53-inducible cell line, TGP53-4, was grown with or without 1 µM doxycycline. To model SIS, primary cells were exposed to 20 µM etoposide.

Transfection, retroviral infection, and SA-β-gal staining

Transfection was performed by using Fugene-HD (Roche) or the calcium phosphate transfection method (Kondoh et al., 2005). EcoPack2-293 (Takara Bio Inc.) packaging cell lines were used for retroviral production. Infected cells were selected by the addition of 75 µg/ml hygromycin, 400 µg/ml (G418), or 2 µg/ml puromycin, as appropriate for the vector. After drug selection, cultures were propagated according to a 3T3 protocol as described previously (Carnero et al., 2000). Cytochemical staining for SA-β-gal was performed at pH 6.0, as described previously (Dimri et al., 1995). The percentage of SA-β-gal–positive cells was determined microscopically by counting the number of positive-staining cells among over 200 cells in total. Images were recorded using a microscope (BZ-9000; KEYENCE) using a 10× 0.45 NA Plan-Apochromat objective lens.

Viability assay

Primary MEFs transfected with various combinations of expression vectors were grown for 24 h and treated with 50 µM etoposide for 24 h. Cells were then collected and stained by trypan blue. Viable cells were counted using a light microscope.

Immunoblotting assay and RNA analysis

For immunoblotting, cell lysates were prepared 24 h after transfection as described previously (Carnero et al., 2000). Cells were washed twice with ice-cold PBS and lysed in lysis buffer (50 mM Tris-HCl, pH 7.5, 200 mM NaCl, 1 mM EDTA, 10% glycerol, 0.5% Triton X-100, 50 mM NaF, 1 mM DTT, 1 mM Na_3VO_4, 1 mM phenylmethanesulfonyl fluoride, and protease inhibitor cocktail; Sigma-Aldrich). After 30 min on ice, lysates were vortexed and cleared by centrifugation. Equivalent amounts of protein were resolved by SDS-PAGE. The antibodies used for immunoblotting and immunostaining are described in the Recombinent proteins and antibodies section.

Total RNA was prepared using the TRIzol reagent (Invitrogen), and cDNA pools were generated using an oligo-dT primer (Promega) and SuperScript III reverse transcription (Invitrogen). Semiquantitative RT-PCR was performed by using a SuperScript one-step RT-PCR kit (Invitrogen) as described previously (Carnero et al., 2000), and real-time PCR was performed using Fast Start Universal SYBR Green Master (Roche). The primers used in these analyses are presented in the Primers section.

Immunoprecipitation

For immunoprecipitation assays, cell lysates were precipitated with the relevant antibody for 2 h. Immune complexes recovered with protein G–agarose beads were washed four times with lysis buffer (50 mM Tris-HCl, pH 7.5, 200 mM NaCl, 1 mM EDTA, 10% glycerol, 0.5% Triton X-100, 50 mM NaF, 1 mM DTT, 1 mM Na_3VO_4, 1 mM phenylmethanesulfonyl fluoride, and protease inhibitor cocktail; Sigma-Aldrich) and boiled in 2× Laemmli sample buffer for 5 min. Denatured immune complexes were resolved on SDS-polyacrylamide gels.

Ubiquitination assays

For detection of ubiquitinated forms of endogenous PGAM, cell extracts were immunoprecipitated with an anti-PGAM antibody, and the precipitated

proteins were denatured and resolved by SDS-PAGE. Ubiquitinated proteins were detected by immunoblotting with an antibody (clone FK2) that detects mono- and polyubiquitinated conjugates.

Detection of proteins labeled with His-tagged ubiquitin was performed as described previously, with modifications (Li et al., 2003). Cells were generally cotransfected with 3 µg of PGAM-FLAG expression plasmid and 3 µg of CMV-driven His-ubiquitin expression plasmid (a gift from T. Matsusaka, The Gurdon Institute, University of Cambridge, Cambridge, UK). After 24–36 h, cells were treated with either 20 µM etoposide for 6 h or exposed to other forms of stress (e.g., Ras-G12V) and treated with MG132. After harvesting, 10% of the cells were processed for direct analysis by immunoblotting while the remainders were used for purification of His-tagged ubiquitinated proteins.

Cell extract was prepared in denaturing conditions by using 6 M guanidine hydrochloride. Cells were resuspended in guanidine lysis buffer (6 M guanidine hydrochloride, 10 mM Tris-Cl, 100 mM Na_2HPO_4, 150 mM NaCl, 0.1% NP-40, and 20 mM imidazole, pH 8.0) at room temperature and sonicated. The lysate was centrifuged at 14,000 *g* for 10 min, and the supernatant was incubated with Ni-NTA beads (QIAGEN) for 2 h at room temperature. The beads were washed five times with guanidine wash buffer (6 M guanidine hydrochloride, 10 mM Tris-Cl, 100 mM Na_2HPO_4, 150 mM NaCl, 0.1% NP-40, and 20 mM imidazole, pH 6.3) at room temperature, followed by five cycles with ice-cold guanidine-free wash buffer (10 mM Tris-Cl, 100 mM Na_2HPO_4, 150 mM NaCl, 0.1% NP-40, and 20 mM imidazole, pH 6.3). His-tagged proteins were eluted from the beads with 50 µl of elution buffer (10 mM Tris-Cl, 100 mM Na_2HPO_4, 150 mM NaCl, 0.1% NP-40, and 250 mM imidazole, pH 6.3). Eluted fractions were analyzed by SDS-PAGE. Ubiquitinated PGAM2-FLAG protein was detected by immunoblotting with anti-FLAG antibody (M2).

In vitro ubiquitination assay

The following GST-tagged recombinant proteins were expressed and purified from *Escherichia coli*: GST-Mdm2-WT, GST-Mdm2-Y281H, GST-Mdm2-W329G, GST-Mdm2-M459I, GST-Mdm2-C464A, GST-p53, GST-PGAM2-WT-FLAG, GST-PGAM2-T2-FLAG, GST-PGAM2-T2-7R-FLAG, GST-PGAM2-TN-FLAG, GST-PGAM2-T4-FLAG, and GST-PGAM2-TC-FLAG. The GST tags were removed from GST fusion proteins by PreScission Protease (GE Healthcare). Other recombinant proteins were purchased: E1 enzyme (UBE1; Boston Biochem), His_6-tagged E2 enzyme (UbcH5b; Enzo Life Sciences), and His_6-tagged ubiquitin (EMD Millipore). In vitro ubiquitination reactions were performed as previously described with some modifications (Li et al., 2003). 35 ng PGAM2-FLAG or p53 was mixed with 100 ng UBE1 (E1), 500 ng UbcH5b (E2), His_6-tagged ubiquitin, and 500 ng Mdm2 (E3). These components were incubated in 30 µl of RXB buffer (40 mM Tris-HCl, pH 7.5, 5 mM $MgCl_2$, 10 mM NaCl, 1 mM DTT, and 2 mM MgATP) for 90 min at 37°C. The ubiquitinated proteins were analyzed by SDS-PAGE and detected by immunoblotting with anti-FLAG (M2) or anti-p53 (DO-1) antibody, respectively.

In vitro kinase assay

Primary MEFs were treated with 20 µM etoposide for 6 h, then lysed with lysis buffer. Endogenous Pak1 proteins were immunoprecipitated from the cell lysates with an anti-Pak1 antibody, and the precipitated proteins were washed twice with Pak1 kinase buffer (100 mM Hepes, 20 mM $MgCl_2$, 4 mM $MnCl_2$, and 0.4 mM dithiothreitol). Equivalent amounts of precipitated protein were incubated with 5 µg of recombinant PGAM2-WT or PGAM2-S118C in 30 µl of Pak1 kinase buffer for 30 min at 30°C in the presence of 10 µCi of γ-[^{32}P]ATP and 10 mM cold ATP. The labeled products were subsequently resolved by SDS-PAGE.

Cycloheximide chase assay

Primary MEFs were cotransfected with plasmids encoding PGAM2-FLAG (WT or S118C mutant) and GFP protein. Transfected cells were treated with 25 µM cycloheximide for 0–120 min. Subsequently, the levels of PGAM2-FLAG and GFP protein were determined by immunoblotting (Ogawara et al., 2002).

Measurement of PGAM activity

PGAM catalytic activity was measured spectrophotometrically as described previously (Kondoh et al., 2005). In brief, samples (20 µg) of cell lysate were incubated with 0.2 mM NADH, 3 mM ADP, 10 µM 2,3-diphosphoglycerate, 600 mU lactate dehydrogenase, 500 mU pyruvate kinase, and 100 mU enolase at 37°C for 10 min. 3-phosphoglyceric acid (3-PGA; 1 mM final concentration) was then added as a substrate. Activity was measured as NAD^+ release over 45 min by monitoring the decrease in absorbance at 340 nm in a Spectra max spectrophotometer (Molecular Devices).

Glycolytic flux measurement

The method used to determine glycolytic flux was based on the metabolism of D-[3-^{3}H] glucose into water after the triose phosphate isomerase reaction. Cells were plated at 0.7 × 10^6 cells per 100-mm dish, and the medium was changed from high glucose (17 mmol/liter) to low glucose (4.25 mmol/liter) 11 h later. D-[3-^{3}H] glucose was added 10 h later. Every 2 h, samples (400 µl) of medium were taken and precipitated with perchloric acid. The supernatant was applied to DOWEX 1X8 200-400 MESH Cl (Sigma-Aldrich) resin after dilution in sodium tetraborate, and the amount of [^{3}H] water in the flow-through was normalized to protein content. Lactate concentration in the culture medium was measured by the lactate assay kit (BioVision), and the value of lactate production was normalized to the protein content of the corresponding cell lysate.

Detection of γ-H2AX foci

Cells plated on coverslips were pre-permeabilized in 0.1% Triton buffer (0.1% [vol/vol] Triton X-100, 20 mM Hepes-KOH, pH 7.4, 50 mM NaCl, 3 mM $MgCl_2$, and 300 mM sucrose) and fixed with 3.7% paraformaldehyde in PBS. The cells were permeabilized with 0.5% Triton buffer (0.5% [vol/vol] Triton X-100, 20 mM Hepes-KOH, pH 7.4, 50 mM NaCl, 3 mM $MgCl_2$, and 300 mM sucrose), followed by treatment with blocking buffer (0.1% skim milk and 0.1% BSA in PBS) and primary antibody solution (anti–γ-H2AX phospho-Ser139 antibody in blocking buffer). After washing with PBS, the coverslips were treated with secondary antibody solution (Alexa Fluor 488 in blocking buffer). Nuclei were stained with DAPI. Images were recorded using a fluorescence microscope (BZ-9000; KEYENCE), using a 40× NA 0.95 Plan-Apochromat objective lens.

Luciferase reporter assay

p53$^{-/-}$*Mdm2*$^{-/-}$ MEFs were transfected with plasmids containing the p21^{CIP1}, Mdm2, or Bax promoter regions upstream of the firefly luciferase reporter in the pGL3 vector (Samuels-Lev et al., 2001), with or without a plasmid encoding wild-type p53, and a renilla luciferase plasmid (pRL-SV40) as a control for transfection efficiency. Cells were harvested 30 h after transfection, and the firefly and renilla luciferase activities were measured using a Dual-Glo Luciferase Assay System (Promega) and a luminometer (Lumat LB9507; BERTHOLD). The levels of firefly luciferase activity were normalized to those of renilla activity.

Soft agar assay

Soft agar assays were performed as described previously (Serrano et al., 1996). Culture dishes (6 cm) were prepared with a bottom layer of 3 ml of DMEM containing 0.4% low-melting agarose. 10^4 cells were mixed with 4 ml of DMEM containing 0.3% low–melting point agarose and seeded on the bottom layer. The colonies were allowed to grow for 2–3 wk and counted by light microscopy.

Nude mouse xenograft assays

8-wk-old nude mice (CAnN.Cg-*Foxn*^{nu}/CrlCrlj; Charles River Laboratories) were injected subcutaneously with 5 × 10^6 cells suspended in 100 µl PBS. Tumor formation was assessed after 3 wk. The procedures for performing animal experiments were in accordance with the principles and guidelines of the Animal Care and Use Committees of Kyoto University Graduate School of Medicine.

Recombinant proteins and antibodies

GST recombinant proteins were expressed in bacteria using pGEX6p-based plasmids. The proteins were purified on glutathione-agarose beads using standard protocols, and the GST tag was removed from the fusion proteins by treatment with PreScission Protease (GE Healthcare). Two rabbits were inoculated with full-length recombinant PGAM2 and the resultant antisera were affinity-purified by reactivity with the recombinant PGAM2.

A phospho-specific antibody against Ser118 of PGAM2 (anti-phospho S118) was generated by injecting rabbits with different synthetic phospho-peptides—B-118P (CVKIWRRS(PO_3)YDVP) and M-118P (CVKIWRRS(PO_3)FDTP)—conjugated to keyhole limpet hemocyanin (KLH) as an adjuvant. Antiserum from one of the four rabbits was found to recognize both phospho-peptides, B-118P and M-118P, but not the unphosphorylated peptides (Fig. S2 A). This rabbit antiserum was affinity purified on an immobilized phospho-peptide column (Thorslund et al., 2007).

Other antibodies used in this study were as follows: anti-FLAG (M2, F3165) from Sigma-Aldrich; anti-HA (12CA5) and anti-GFP from Roche; anti–c-Myc (9E10), anti-actin (C-11), anti-Pak1 (N-20), anti–human p53 (DO-1), anti-p21^{CIP1} (C-19), and anti-p16^{INK4} (M156) from Santa Cruz Biotechnology, Inc.; anti–mouse p53 (pAb421) from EMD Millipore; anti-Mdm2

(2A10) and anti-PGK from Abcam; anti-GAPDH (6C5) from EMD Millipore; anti-Enolase from BD; anti-PFK (C-terminal L684) from Abgent; anti-phospho Ser1981 ATM (10H11.E12) from Rockland Immunochemicals Inc.; anti–γ-H2AX (phosphor-Ser139 antibody; ab2893) from Abcam; Alexa Fluor 488 (A11070) from Invitrogen; and anti–mono- and polyubiquitinated conjugates antibody (clone FK2) from Enzo Life Sciences.

Plasmid DNAs

pHygro Marx II retroviral vectors encoding mouse *PGAM1* or *PGAM2* have been described previously (Kondoh et al., 2005). Expression of full-length *PGAM1* and *PGAM2* with no tag was driven by retroviral LTR promoter of pHygro Marx II. Human *PGAM1* cDNA was generated by RT-PCR from cell RNA and cloned into the pWZL neo retroviral vector. The human PGAM2 expression plasmid was a gift from Y. Yoshida (Center for iPS Cell Research and Application [CiRA], Kyoto University, Kyoto, Japan). Site-directed mutations in *PGAM2* were generated by PCR-based mutagenesis as described previously. The relevant variants of *PGAM2* are as follows: PGAM2-S118C, PGAM2-S118D, PGAM2-S118A, PGAM2-4R, and PGAM2-7R. Deletion mutants of mouse *PGAM2* cDNA were also generated by PCR, including PGAM-T1, PGAM-T2, PGAM-T3, PGAM-TN, PGAM-T4, and PGAM-TC. The different variants of *PGAM2* cDNA, and the wild-type PGAM1-WT and PGAM2-WT, were subcloned into the p3×FLAG-CMV14 expression vector. To produce recombinant proteins in bacteria, wild-type *PGAM2* and the PGAM2-S118C mutant cDNAs were transferred into the pGEX6p expression vector. HA-tagged *Pak1* cDNA was subcloned into a retroviral WZL-neo vector. The kinase-defective mutant Pak1-K299R (Zhang et al., 1995) was generated by PCR-based mutagenesis. To produce shRNAs against mouse *Pak1*, the relevant DNA oligonucleotides were annealed and ligated into the HindIII and BglII sites of the pRETRO-SUPER vector (Oligoengine; Brummelkamp et al., 2002). The pCMV-Myc vector containing human *Mdm2* cDNA has been described previously. Substitution mutants of *Mdm2* (Y281H, W329G, M459I) were generated by PCR-based mutagenesis. The CMV-driven human Mdm2 C464A expression plasmid was a gift from K.H. Vousden (Cancer Research UK, Beatson Institute, London, England, UK). The variants of *Mdm2* cDNA were cloned into the pCMV-Myc vector or the WZL-neo retroviral vector. For the in vitro ubiquitination assay, the variants of 3×FLAG-tagged *PGAM2* cDNA, including PGAM2-T2, -T2-7R, -TN, -T4, and -TC, were subcloned into the pGEX6p vector. Similarly, the various forms of human *Mdm2* (WT, Y281H, W329G, M459I, and C464A) and *p53* were subcloned into pGEX6p. The pBabe-puro-Ras-G12V plasmid was a gift from K. Maehara (National Center for Child Health and Development, Tokyo, Japan). To generate *PGAM2* transgenic mice, FLAG-tagged *PGAM2* was cloned into the pCAGGS vector. The pGAGGS plasmid was a gift from J.-i. Miyazaki (Division of Stem Cell Regulation Research, Osaka University Graduate School of Medicine, Osaka, Japan). The primer sequences used in this study are presented below.

cDNA

Accession numbers of cDNA (available from GenBank) used in this study were as follows: mouse *PGAM1*, NM_023418; mouse *PGAM2*, NM_018870; human *PGAM1*, NM_002629; human *PGAM2*, NM_013016; rat *Pak1*, NM_017198; human *Mdm2*, NM_00239.5.

Primers used for subcloning of *PGAM1* (PGM-B) and *PGAM2* (PGM-M) cDNA. PGM-M forward (Fw), 5′-AAGAATTCATGACCACCCACCGCCTAG-3′; PGM-M reverse (Re), 5′-ATATGGATCCTGGCTTCGCCTTTCCCTGGGCA-3′; PGM-B Fw, 5′-ATATGAATTCATGGCTGCCTACAAGCTGGT-3′; PGM-B Re, 5′-ATATGGATCCTGGCTTCTTCACCTTGCCCTGAG-3′; hPGM-B Fw, 5′-ATATGGGATCCGCCACCATGGCCGCCTACAAACTGGTG-3′; hPGM-B Re, 5′-ATATGAATTCTCACTTCTTGGCCTTGCCCTGG-3′.

Primers used for mutagenesis of *PGAM2* cDNA. PGM-M Fw, 5′-AAGAATTCATGACCACCCACCGCCTAG-3′; PGM-M Re, 5′-ATATGGATCCTGGCTTCGCCTTTCCCTGGGCA-3′; S118C Fw (mutation site F), 5′-CAGGTGAAGATCTGGAGGCGTTGCTTTGACACCCCACCACCACCC-3′; S118C Re (mutation site R), 5′-GGGTGGTGGTGGGGTGTCAAAGCAACGCCTCCAGATCTTCACCTGCTC-3′; S118A Fw (mutation site F), 5′-CAGGTGAAGATCTGGAGGCGTGCCTTTGACACCCCACCACCACCC-3′; S118A Re (mutation site R), 5′-GGGTGGTGGTGGGGTGTCAAAGGCACGCCTCCAGATCTTCACCTG-3′; S118D Fw (mutation site F), 5′-CAGGTGAAGATCTGGAGGCGTGACTTTGACACCCCACCACCACCC-3′; S118D Re (mutation site R), 5′-GGGTGGTGGTGGGGTGTCAAAGTCACGCCTCCAGATCTTCACCTGCTC-3′; 4R-1 Fw (mutation site F), 5′-CCATGGAAGAGAAACACAACTACTACACCTCCATCAGCAGGGACCGC-3′; 4R-1 Re (mutation site R), 5′-GCGGTCCCTGCTGATGGAGGTGTAGTAGTTGTGTTTCTCTTCCATGG-3′; 4R-2 Fw (mutation site F), 5′-GAGACGGCTGCAAGGCACGGGGAGGAGCAGGTGAGGATCTGGAGGCG-3′; 4R-2 Re (mutation site R), 5′-CGCCTCCAGATCCTCACCTGCTCCTCCCCGTGCCTTGCAGCCGTCTC-3′; 7R-1 Fw (mutation site F), 5′-GTGGCCTCACAGGCCTCAATAGGGCTGAGACGGCTGCAAGGCACGGG-3′; 7R-1 Re (mutation site R), 5′-CCCGTGCCTTGCAGCCGTCTCAGCCCTATTGAGGCCTGTGAGGCCAC-3′; 7R-2 Fw (mutation site F), 5′-GGCTTGAGGCCTGAGGAGCTGCCTACCTGTGAAAGTCTCAGGGACAC-3′; 7R-2 Re (mutation site R), 5′-GTGTCCCTGAGACTTTCACAGGTAGGCAGCTCCTCAGGCCTCAAGCC-3′.

Primers used to generate deleted versions of *PGAM2* cDNA. Pgam2F, 5′-CCGAATTCATGACCACCCACCGCCTAGT-3′; F1, 5′-CCGAATTCATGGTGGTGCGTACCTGGC-3′; R1, 5′-CCGATATCCTTCGCCTTTCCCTGGGCAGC-3′; F2, 5′-CGGAATTCATGAAGATTAAGGCTGCCAGAGAG-3′; R2, 5′-CCGATATCAGGTGCGATCTCCTCATTCC-3′; R3, 5′-GTGATATCGGGCACCCACACATTTGGTC-3′. Pgam2F and R1 were used for PCR of PGAM2-T1 cloning. F1 and R1 were used for PCR of PGAM2-T2 cloning. Pgam2F and R2 were used for PCR of PGAM2-T3 cloning. Pgam2F and R3 were used for PCR of PGAM2-TN cloning. F1 and R2 were used for PCR of PGAM2-T4 cloning. F2 and R1 were used for PCR of PGAM2-TC cloning.

Primers used for mutagenesis of *Mdm2* cDNA. Mdm2 Fw (mutation site F), 5′-ATAGAATTCTGGTGAGGAGCAGGCAA-3′; Mdm2 Re (mutation site R), 5′-TATCTCGAGCTAGGGGAAATAAGTTAGCAC-3′; Y281H Fw (mutation site F), 5′-GATGAGGTATATCAAGTTACTGTGCATCAGGCAGGGGAGAGTGATAC-3′; Y281H Re (mutation site R), 5′-GTATCACTCTCCCCTGCCTGATGCACAGTAACTTGATATACCTCATC-3′; W329G Fw (mutation site F), 5′-GATGTTGGGCCCTTCGTGAGAATGGGCTTCCTGAAGATAAAGGGAAAG-3′; W329G Re (mutation site R), 5′-CTTTCCCTTTATCTTCAGGAAGCCCATTCTCACGAAGGGCCCAACATC-3′; M459I Fw (mutation site F), 5′-CATGGCAAAACAGGACATCTTATTGCCTGCTTTACATGTGCAAAGAAG-3′; M459I Re (mutation site R), 5′-CTTCTTTGCACATGTAAAGCAGGCAATAAGATGTCCTGTTTTGCCATG-3′.

Primers used for mutagenesis of *Pak1* cDNA. Pak1 Fw (mutation site F), 5′-ATATGAATTCACCATGTACCCATACGACGTG-3′; Pak1 Re (mutation site R), 5′-ATATGAATTCTCAGTGATTGTTCTTGGTTGCC-3′; K299R Fw (mutation site F), 5′-ACAGGGCAGGAGGTGGCCATTAGACAGATGAACCTTCAGCAGCAG-3′; K299R Re (mutation site R), 5′-CTGCTGCTGAAGGTTCATCTGTCTAATGGCCACCTCCTGCCCTGT-3′.

Primers used to generate *Pak1* shRNA. shPak1 no. 1 Fw, 5′-GATCCCCGTACACACGGTTCGAGAAGTTCAAGAGACTTCTCGAACCGTGTGTACTTTTTGGAAA-3′; shPak1 no. 1 Re, 5′-AGCTTTTCCAAAAAGTACACGGTTCGAGAAGTCTCTTGAACTTCTCGAACCGTGTGTACGGG-3′; shPak1 No. 2 Fw, 5′-GATCCCCCCCTAAACCAGGGCTCCAATTCAAGAGATTGGAGCCGTGGTTTAGGGTTTTTGGAAA-3′; shPak1 No. 2 Re, 5′-AGCTTTTCCAAAAACCCTAAACCACGGCTCCAATCTCTTGAATTGGAGCCGTGGTTTAGGGG-3′.

Primers used to generate the *PGAM2* transgene in mice. Forward, 5′-ATATGAATTCATGACCACCCACCGCCTAGT-3′; reverse, 5′-ATATGAATTCCTACTTGTCATCGTCATCCT-3′.

Primers used for semi-quantitative RT-PCR. Mouse PGAM1 Fw, 5′-GAACTGTGCTGTGGTGTGACC-3′; mouse PGAM1 Re, 5′-AGCTCTGAACCCACACGGTAG-3′; mouse PGAM2 Fw, 5′-GGCTTGAAGCCTGAGGAGCTG-3′; mouse PGAM2 Re, 5′-AACTTTATTGCCCCGTCCACC-3′; mouse β-actin Fw, 5′-AGGCTCTTTTCCAGCCTTCCT-3′; mouse β-actin Re, 5′-ATAAGAGACAACATTGGCATGGC-3′.

Primers used for real-time qRT-PCR analysis. Mouse PGAM1-qRT Fw, 5′-GTTGCGAGATGCTGGCTATGA-3′; mouse PGAM1-qRT Re, 5′-CACATCTGGTCAATGGCATCC-3′; mouse PGAM2-qRT Fw, 5′-TGGAATGAGGAGATCGCACCT-3′; mouse PGAM2-qRT Re, 5′-TCGGACATCCCTTCCAGATGT-3′; mouse β-actin-qRT Fw, 5′-CGTGCGTGACATCAAAGAGAA-3′; mouse β-actin-qRT Re, 5′-AACCGCTCGTTGCCAATAGT-3′; mouse Mdm2-qRT Fw, 5′-GAAGATGCGCGGGAAGTAG-3′; mouse Mdm2-qRT Re, 5′-CATGTTGGTATTGCACATTGG-3′; mouse p53-qRT Fw, 5′-CTAGCATTCAGGCCCTCATC-3′; mouse p53-qRT Re, 5′-TCCGACTGTGACTCCTCCAT-3′; mouse Pak1-qRT Fw, 5′-AACCCAGAGAAGTTGTCAGC-3′; mouse Pak1-qRT Re, 5′-CAATCAGTGGAGTCAGGCTAG-3′; mouse RPL13-qRT Fw, 5′-TGCTGCTCTCAAGGTTGTTCG-3′; mouse RPL13-qRT Re, 5′-GCCTTTTCCTTCCGTTTCTCC-3′.

Statistical analysis

All data, without Fig. 8 H, are expressed as the mean ± SEM of three independent experiments. Comparisons between groups were analyzed with *t* tests.

Online supplemental material

Fig. S1 shows detection of PGAM1 and -2 and validation of the anti-PGAM polyclonal antibody. Fig. S2 shows that Pak1 promotes phosphorylation and

ubiquitination of PGAM. Fig. S3 shows effects of p53 and Mdm2 on PGAM protein levels. Fig. S4 shows ubiquitination of PGAM2 in vitro and mutation of relevant lysine residues. Fig. S5 shows that Mdm2-M459I affects ubiquitination of both PGAM and p53. Online supplemental material is available at http://www.jcb.org/cgi/content/full/jcb.201306149/DC1.

We thank the staff in the Geriatric Department of Kyoto University for cooperation; Eri Shibata and Setsuo Asahi for providing excellent technical assistance; and Dr. Kayoko Maehara, Dr. Takahiro Matsusaka, Dr. Karen H. Vousden, Dr. Yoshinori Yoshida, and Dr. Jun-ichi Miyazaki for providing experimental materials. The animal experiment and the radio isotope experiment were performed at the institute of Laboratory Animals, Graduate School of Medicine, Kyoto University, and in the Kyoto University Hospital Radioisotopes Research Laboratory, respectively.

T. Maruyama was supported by a postdoctoral fellowship from the Global COE program "Center for Frontier Medicine." This work was supported in part by grants from the Global COE program "Center for Frontier Medicine," from the Japan Society for the Promotion of Science, from the Ministry of Education, Culture, Sports, Science, and Technology of Japan (grants No. 20590696 and No. 23390186), from the Japan Science and Technology Agency (grants No. 8447 and No. 5485), and from Japan Science and Technology Agency (JST) Core Research for Evolutional Science and Technology (CREST No. 18 to H. Kondoh).

The authors declare no competing financial interests.

Submitted: 26 June 2013
Accepted: 10 January 2014

References

Acosta, J.C., A. O'Loghlen, A. Banito, M.V. Guijarro, A. Augert, S. Raguz, M. Fumagalli, M. Da Costa, C. Brown, N. Popov, et al. 2008. Chemokine signaling via the CXCR2 receptor reinforces senescence. *Cell*. 133:1006–1018. http://dx.doi.org/10.1016/j.cell.2008.03.038

Bensaad, K., A. Tsuruta, M.A. Selak, M.N. Vidal, K. Nakano, R. Bartrons, E. Gottlieb, and K.H. Vousden. 2006. TIGAR, a p53-inducible regulator of glycolysis and apoptosis. *Cell*. 126:107–120. http://dx.doi.org/10.1016/j.cell.2006.05.036

Brown, D.R., C.A. Thomas, and S.P. Deb. 1998. The human oncoprotein MDM2 arrests the cell cycle: elimination of its cell-cycle-inhibitory function induces tumorigenesis. *EMBO J.* 17:2513–2525. http://dx.doi.org/10.1093/emboj/17.9.2513

Brummelkamp, T.R., R. Bernards, and R. Agami. 2002. A system for stable expression of short interfering RNAs in mammalian cells. *Science*. 296:550–553. http://dx.doi.org/10.1126/science.1068999

Campisi, J. 2013. Aging, cellular senescence, and cancer. *Annu. Rev. Physiol.* 75:685–705. http://dx.doi.org/10.1146/annurev-physiol-030212-183653

Cancer Genome Atlas Research Network. 2008. Comprehensive genomic characterization defines human glioblastoma genes and core pathways. *Nature*. 455:1061–1068. http://dx.doi.org/10.1038/nature07385

Carnero, A., J.D. Hudson, C.M. Price, and D.H. Beach. 2000. p16INK4A and p19ARF act in overlapping pathways in cellular immortalization. *Nat. Cell Biol.* 2:148–155.

Chen, Q., and B.N. Ames. 1994. Senescence-like growth arrest induced by hydrogen peroxide in human diploid fibroblast F65 cells. *Proc. Natl. Acad. Sci. USA*. 91:4130–4134. http://dx.doi.org/10.1073/pnas.91.10.4130

Dimri, G.P., X. Lee, G. Basile, M. Acosta, G. Scott, C. Roskelley, E.E. Medrano, M. Linskens, I. Rubelj, O. Pereira-Smith, et al. 1995. A biomarker that identifies senescent human cells in culture and in aging skin in vivo. *Proc. Natl. Acad. Sci. USA*. 92:9363–9367. http://dx.doi.org/10.1073/pnas.92.20.9363

Ding, L., G. Getz, D.A. Wheeler, E.R. Mardis, M.D. McLellan, K. Cibulskis, C. Sougnez, H. Greulich, D.M. Muzny, M.B. Morgan, et al. 2008. Somatic mutations affect key pathways in lung adenocarcinoma. *Nature*. 455:1069–1075. http://dx.doi.org/10.1038/nature07423

Durany, N., J. Joseph, E. Campo, R. Molina, and J. Carreras. 1997. Phosphoglycerate mutase, 2,3-bisphosphoglycerate phosphatase and enolase activity and isoenzymes in lung, colon and liver carcinomas. *Br. J. Cancer*. 75:969–977. http://dx.doi.org/10.1038/bjc.1997.168

Durany, N., J. Joseph, O.M. Jimenez, F. Climent, P.L. Fernández, F. Rivera, and J. Carreras. 2000. Phosphoglycerate mutase, 2,3-bisphosphoglycerate phosphatase, creatine kinase and enolase activity and isoenzymes in breast carcinoma. *Br. J. Cancer*. 82:20–27.

Evans, M.J., A. Saghatelian, E.J. Sorensen, and B.F. Cravatt. 2005. Target discovery in small-molecule cell-based screens by in situ proteome reactivity profiling. *Nat. Biotechnol.* 23:1303–1307. http://dx.doi.org/10.1038/nbt1149

Hagai, T., A. Tóth-Petróczy, A. Azia, and Y. Levy. 2012. The origins and evolution of ubiquitination sites. *Mol. Biosyst.* 8:1865–1877. http://dx.doi.org/10.1039/c2mb25052g

Haupt, Y., R. Maya, A. Kazaz, and M. Oren. 1997. Mdm2 promotes the rapid degradation of p53. *Nature*. 387:296–299. http://dx.doi.org/10.1038/387296a0

Hayflick, L. 1965. The limited in vitro lifetime of human diploid cell strains. *Exp. Cell Res.* 37:614–636. http://dx.doi.org/10.1016/0014-4827(65)90211-9

Hershko, A., and A. Ciechanover. 1998. The ubiquitin system. *Annu. Rev. Biochem.* 67:425–479. http://dx.doi.org/10.1146/annurev.biochem.67.1.425

Hitosugi, T., L. Zhou, S. Elf, J. Fan, H.B. Kang, J.H. Seo, C. Shan, Q. Dai, L. Zhang, J. Xie, et al. 2012. Phosphoglycerate mutase 1 coordinates glycolysis and biosynthesis to promote tumor growth. *Cancer Cell*. 22:585–600. http://dx.doi.org/10.1016/j.ccr.2012.09.020

International Cancer Genome Consortium. 2010. International network of cancer genome projects. *Nature*. 464:993–998. (published erratum appears in *Nature*. 2010. 17:465) http://dx.doi.org/10.1038/nature08987

Itahana, K., H. Mao, A. Jin, Y. Itahana, H.V. Clegg, M.S. Lindström, K.P. Bhat, V.L. Godfrey, G.I. Evan, and Y. Zhang. 2007. Targeted inactivation of Mdm2 RING finger E3 ubiquitin ligase activity in the mouse reveals mechanistic insights into p53 regulation. *Cancer Cell*. 12:355–366. http://dx.doi.org/10.1016/j.ccr.2007.09.007

Iyer, N.V., L.E. Kotch, F. Agani, S.W. Leung, E. Laughner, R.H. Wenger, M. Gassmann, J.D. Gearhart, A.M. Lawler, A.Y. Yu, and G.L. Semenza. 1998. Cellular and developmental control of O2 homeostasis by hypoxia-inducible factor 1 alpha. *Genes Dev.* 12:149–162. http://dx.doi.org/10.1101/gad.12.2.149

Jones, R.G., D.R. Plas, S. Kubek, M. Buzzai, J. Mu, Y. Xu, M.J. Birnbaum, and C.B. Thompson. 2005. AMP-activated protein kinase induces a p53-dependent metabolic checkpoint. *Mol. Cell*. 18:283–293. http://dx.doi.org/10.1016/j.molcel.2005.03.027

Kawauchi, K., K. Araki, K. Tobiume, and N. Tanaka. 2008. p53 regulates glucose metabolism through an IKK-NF-κB pathway and inhibits cell transformation. *Nat. Cell Biol.* 10:611–618. http://dx.doi.org/10.1038/ncb1724

Kondoh, H., M.E. Lleonart, J. Gil, J. Wang, P. Degan, G. Peters, D. Martinez, A. Carnero, and D. Beach. 2005. Glycolytic enzymes can modulate cellular life span. *Cancer Res.* 65:177–185.

Koppenol, W.H., P.L. Bounds, and C.V. Dang. 2011. Otto Warburg's contributions to current concepts of cancer metabolism. *Nat. Rev. Cancer*. 11:325–337. http://dx.doi.org/10.1038/nrc3038

Kubbutat, M.H., S.N. Jones, and K.H. Vousden. 1997. Regulation of p53 stability by Mdm2. *Nature*. 387:299–303. http://dx.doi.org/10.1038/387299a0

Kubbutat, M.H., R.L. Ludwig, A.J. Levine, and K.H. Vousden. 1999. Analysis of the degradation function of Mdm2. *Cell Growth Differ.* 10:87–92.

Kuilman, T., C. Michaloglou, L.C. Vredeveld, S. Douma, R. van Doorn, C.J. Desmet, L.A. Aarden, W.J. Mooi, and D.S. Peeper. 2008. Oncogene-induced senescence relayed by an interleukin-dependent inflammatory network. *Cell*. 133:1019–1031. http://dx.doi.org/10.1016/j.cell.2008.03.039

Leach, F.S., T. Tokino, P. Meltzer, M. Burrell, J.D. Oliner, S. Smith, D.E. Hill, D. Sidransky, K.W. Kinzler, and B. Vogelstein. 1993. p53 Mutation and MDM2 amplification in human soft tissue sarcomas. *Cancer Res.* 53:2231–2234.

Li, M., C.L. Brooks, F. Wu-Baer, D. Chen, R. Baer, and W. Gu. 2003. Mono- versus polyubiquitination: differential control of p53 fate by Mdm2. *Science*. 302:1972–1975. http://dx.doi.org/10.1126/science.1091362

Lipkowitz, S., and A.M. Weissman. 2011. RINGs of good and evil: RING finger ubiquitin ligases at the crossroads of tumour suppression and oncogenesis. *Nat. Rev. Cancer*. 11:629–643. http://dx.doi.org/10.1038/nrc3120

Manfredi, J.J. 2010. The Mdm2-p53 relationship evolves: Mdm2 swings both ways as an oncogene and a tumor suppressor. *Genes Dev.* 24:1580–1589. http://dx.doi.org/10.1101/gad.1941710

McClatchey, A.I., I. Saotome, K. Mercer, D. Crowley, J.F. Gusella, R.T. Bronson, and T. Jacks. 1998. Mice heterozygous for a mutation at the Nf2 tumor suppressor locus develop a range of highly metastatic tumors. *Genes Dev.* 12:1121–1133. http://dx.doi.org/10.1101/gad.12.8.1121

Molli, P.R., D.Q. Li, B.W. Murray, S.K. Rayala, and R. Kumar. 2009. PAK signaling in oncogenesis. *Oncogene*. 28:2545–2555. http://dx.doi.org/10.1038/onc.2009.119

Niwa, H., K. Yamamura, and J. Miyazaki. 1991. Efficient selection for high-expression transfectants with a novel eukaryotic vector. *Gene*. 108:193–199. http://dx.doi.org/10.1016/0378-1119(91)90434-D

Ogawara, Y., S. Kishishita, T. Obata, Y. Isazawa, T. Suzuki, K. Tanaka, N. Masuyama, and Y. Gotoh. 2002. Akt enhances Mdm2-mediated ubiquitination and degradation of p53. *J. Biol. Chem.* 277:21843–21850. http://dx.doi.org/10.1074/jbc.M109745200

Osthus, R.C., H. Shim, S. Kim, Q. Li, R. Reddy, M. Mukherjee, Y. Xu, D. Wonsey, L.A. Lee, and C.V. Dang. 2000. Deregulation of glucose transporter 1 and glycolytic gene expression by c-Myc. *J. Biol. Chem.* 275:21797–21800. http://dx.doi.org/10.1074/jbc.C000023200

Parrinello, S., E. Samper, A. Krtolica, J. Goldstein, S. Melov, and J. Campisi. 2003. Oxygen sensitivity severely limits the replicative lifespan of murine fibroblasts. *Nat. Cell Biol.* 5:741–747. http://dx.doi.org/10.1038/ncb1024

Poyurovsky, M.V., X. Jacq, C. Ma, O. Karni-Schmidt, P.J. Parker, M. Chalfie, J.L. Manley, and C. Prives. 2003. Nucleotide binding by the Mdm2 RING domain facilitates Arf-independent Mdm2 nucleolar localization. *Mol. Cell*. 12:875–887. http://dx.doi.org/10.1016/S1097-2765(03)00400-3

Prives, C. 1998. Signaling to p53: breaking the MDM2-p53 circuit. *Cell*. 95:5–8. http://dx.doi.org/10.1016/S0092-8674(00)81774-2

Reifenberger, G., L. Liu, K. Ichimura, E.E. Schmidt, and V.P. Collins. 1993. Amplification and overexpression of the MDM2 gene in a subset of human malignant gliomas without p53 mutations. *Cancer Res.* 53:2736–2739.

Ren, F., H. Wu, Y. Lei, H. Zhang, R. Liu, Y. Zhao, X. Chen, D. Zeng, A. Tong, L. Chen, et al. 2010. Quantitative proteomics identification of phosphoglycerate mutase 1 as a novel therapeutic target in hepatocellular carcinoma. *Mol. Cancer*. 9:81. http://dx.doi.org/10.1186/1476-4598-9-81

Rodrigues, N.R., A. Rowan, M.E. Smith, I.B. Kerr, W.F. Bodmer, J.V. Gannon, and D.P. Lane. 1990. p53 mutations in colorectal cancer. *Proc. Natl. Acad. Sci. USA*. 87:7555–7559. http://dx.doi.org/10.1073/pnas.87.19.7555

Ruiz-Lozano, P., M.L. Hixon, M.W. Wagner, A.I. Flores, S. Ikawa, A.S. Baldwin Jr., K.R. Chien, and A. Gualberto. 1999. p53 is a transcriptional activator of the muscle-specific phosphoglycerate mutase gene and contributes in vivo to the control of its cardiac expression. *Cell Growth Differ.* 10:295–306.

Samuels-Lev, Y., D.J. O'Connor, D. Bergamaschi, G. Trigiante, J.K. Hsieh, S. Zhong, I. Campargue, L. Naumovski, T. Crook, and X. Lu. 2001. ASPP proteins specifically stimulate the apoptotic function of p53. *Mol. Cell*. 8:781–794. http://dx.doi.org/10.1016/S1097-2765(01)00367-7

Schraml, P., G. Schwerdtfeger, F. Burkhalter, A. Raggi, D. Schmidt, T. Ruffalo, W. King, K. Wilber, M.J. Mihatsch, and H. Moch. 2003. Combined array comparative genomic hybridization and tissue microarray analysis suggest PAK1 at 11q13.5-q14 as a critical oncogene target in ovarian carcinoma. *Am. J. Pathol.* 163:985–992. http://dx.doi.org/10.1016/S0002-9440(10)63458-X

Seger, Y.R., M. García-Cao, S. Piccinin, C.L. Cunsolo, C. Doglioni, M.A. Blasco, G.J. Hannon, and R. Maestro. 2002. Transformation of normal human cells in the absence of telomerase activation. *Cancer Cell*. 2:401–413. http://dx.doi.org/10.1016/S1535-6108(02)00183-6

Serrano, M., H. Lee, L. Chin, C. Cordon-Cardo, D. Beach, and R.A. DePinho. 1996. Role of the INK4a locus in tumor suppression and cell mortality. *Cell*. 85:27–37. http://dx.doi.org/10.1016/S0092-8674(00)81079-X

Serrano, M., A.W. Lin, M.E. McCurrach, D. Beach, and S.W. Lowe. 1997. Oncogenic ras provokes premature cell senescence associated with accumulation of p53 and p16INK4a. *Cell*. 88:593–602. http://dx.doi.org/10.1016/S0092-8674(00)81902-9

Shalom-Barak, T., and U.G. Knaus. 2002. A p21-activated kinase-controlled metabolic switch up-regulates phagocyte NADPH oxidase. *J. Biol. Chem.* 277:40659–40665. http://dx.doi.org/10.1074/jbc.M206650200

Terzian, T., Y.A. Suh, T. Iwakuma, S.M. Post, M. Neumann, G.A. Lang, C.S. Van Pelt, and G. Lozano. 2008. The inherent instability of mutant p53 is alleviated by Mdm2 or p16INK4a loss. *Genes Dev.* 22:1337–1344. http://dx.doi.org/10.1101/gad.1662908

Thorslund, T., F. Esashi, and S.C. West. 2007. Interactions between human BRCA2 protein and the meiosis-specific recombinase DMC1. *EMBO J.* 26:2915–2922. http://dx.doi.org/10.1038/sj.emboj.7601739

Vadlamudi, R.K., L. Adam, R.A. Wang, M. Mandal, D. Nguyen, A. Sahin, J. Chernoff, M.C. Hung, and R. Kumar. 2000. Regulatable expression of p21-activated kinase-1 promotes anchorage-independent growth and abnormal organization of mitotic spindles in human epithelial breast cancer cells. *J. Biol. Chem.* 275:36238–36244. http://dx.doi.org/10.1074/jbc.M002138200

Vander Heiden, M.G., L.C. Cantley, and C.B. Thompson. 2009. Understanding the Warburg effect: the metabolic requirements of cell proliferation. *Science*. 324:1029–1033. http://dx.doi.org/10.1126/science.1160809

Vander Heiden, M.G., J.W. Locasale, K.D. Swanson, H. Sharfi, G.J. Heffron, D. Amador-Noguez, H.R. Christofk, G. Wagner, J.D. Rabinowitz, J.M. Asara, and L.C. Cantley. 2010. Evidence for an alternative glycolytic pathway in rapidly proliferating cells. *Science*. 329:1492–1499. http://dx.doi.org/10.1126/science.1188015

Wang, R.A., A. Mazumdar, R.K. Vadlamudi, and R. Kumar. 2002. P21-activated kinase-1 phosphorylates and transactivates estrogen receptor-α and promotes hyperplasia in mammary epithelium. *EMBO J.* 21:5437–5447. http://dx.doi.org/10.1093/emboj/cdf543

Warburg, O. 1956. On respiratory impairment in cancer cells. *Science*. 124:269–270.

Zhang, S., J. Han, M.A. Sells, J. Chernoff, U.G. Knaus, R.J. Ulevitch, and G.M. Bokoch. 1995. Rho family GTPases regulate p38 mitogen-activated protein kinase through the downstream mediator Pak1. *J. Biol. Chem.* 270:23934–23936. http://dx.doi.org/10.1074/jbc.270.41.23934

Zhang, J., L. Yu, Q. Fu, J. Gao, Y. Xie, J. Chen, P. Zhang, Q. Liu, and S. Zhao. 2001. Mouse phosphoglycerate mutase M and B isozymes: cDNA cloning, enzyme activity assay and mapping. *Gene*. 264:273–279. http://dx.doi.org/10.1016/S0378-1119(00)00597-7

Zwerschke, W., S. Mazurek, P. Stöckl, E. Hütter, E. Eigenbrodt, and P. Jansen-Dürr. 2003. Metabolic analysis of senescent human fibroblasts reveals a role for AMP in cellular senescence. *Biochem. J.* 376:403–411. http://dx.doi.org/10.1042/BJ20030816